Bioelectric Modulation of Fate Decisions in Mesenchymal Stem Cells

An Honors Thesis for the Department of Biology at Tufts University

Thesis Advisor: Dr. Michael Levin
Mentor: Dr. Juanita Mathews

Ben Cooper
2019

Table of Contents

Acknowledgements

Mike Levin inspired my interest in biology with a guest lecture in one of my psych classes that brought to my attention some of the incredible biological phenomena that are still incompletely understood and that, as an organism myself, I had taken for granted. I was thrilled when a spot opened up in his lab a year later, and I'll always be grateful that Mike takes the time to speak to undergrads and ultimately shaped my undergraduate experience. Mike's time is often in high demand, and I was amazed by how much he offered to me and everyone else, even accommodating my last-minute cramming!

My mentor Juanita Mathews stayed patient and taught me basically everything that I know how to do in the lab. There have been plenty of ups and downs, but I can't express enough thanks to her for having stayed so encouraging and available despite some dramatic changes in her personal life, even texting me advice the night that she gave birth to her daughter and writing me a recommendation from the hospital. I'm extremely grateful for the opportunity and guidance that both Mike and Juanita have provided.

I'm also, of course, grateful for many other Levin lab members. Joel's microfluidics chips were central to my research. Sophia made a last-minute push to try to get me patch clamp data. Nirosha, Amar, and Gizem all made themselves available to answer my questions and offer support during Juanita's leave, and Josh and Jayati provided a constant flow of logistical support without which I would have been helpless. I'm also thankful to everyone else in the lab who created such a relaxed and constructive work environment, and I can't wait to be back next year!

Finally, I'm thankful for the rest of the Tufts biology department staff and faculty, including my third thesis committee member Kelly McLaughlin and major advisor Mitch McVey, who helped provide me with a great undergraduate experience.

Abstract

Every organism starts as a single totipotent stem cell, capable of giving rise to all cell types. As this cell and its progeny proliferate, migrate, and differentiate, they are exposed to a wide array of signals and must in turn make a coordinated effort to generate tissues, organs, and bodies. Of these various signaling modalities, endogenous cell to cell electrical signaling and the resulting bioelectric dynamics have been shown regulate numerous developmental processes, and this signaling is tractable. Previous work has demonstrated that stem cells can be moved forwards or backwards along the spectrum of a given cell lineage by sustained changes to their membrane potentials. However, it is still unknown whether or not bioelectricity can control *which* fate stem cells will choose. Due to the growing number of known influences on stem cell differentiation and the role of bioelectricity in controlling the identity of biological systems, we hypothesized that bioelectricity is a medium through which various, potentially ambiguous signals are integrated and distributed such that stem cells can make a unified decision to generate a given tissue. Here, using mesenchymal stem cells (MSCs), we first created a toolbox of transgenic fluorescent reporter MSC lines that enable the long-term, real-time measurement of changes to bioelectric patterns and gene expression during differentiation. We then investigated the role of bioelectricity in stem cell fate choice by exposing MSCs to a bipotential medium capable of inducing both adipogenesis and osteogenesis along with ion channel and gap junction modulators. We found that inhibition of gap junction intercellular communication enhances osteogenesis and that hyperpolarization non-uniformly alters MSC fate choice in manner that is dependent on the nature of the hyperpolarization. These results are promising indicators that stem cell fate choice can be bioelectrically manipulated, which calls for further investigation into the topic using more precise methods.

Introduction

Stem cells' ability to generate tissues through self-renewal and differentiation make them an exciting prospect for synthetic biology, regenerative medicine, and biological systems modeling. To capitalize on this potential, further understanding the control points of stem cell behavior and differentiation is paramount. Biochemical signaling is the most well characterized method of directing stem cell differentiation (Hwang et al., 2007; Li et al., 2013; Zhu et al., 2011), but there is growing evidence that differentiation is driven by a complex interplay of biochemical and biophysical signaling modalities (Sun et al., 2012).

One such biophysical signaling modality is bioelectricity (Levin et al., 2017; Levin and Martyniuk, 2018), consisting of endogenous ion currents and long-term transmembrane potential (V_{mem}) profiles that are determined by differences in the concentrations of charged molecules and ions inside and outside of the cell. A fundamental component of bioelectricity is its capacity to propagate throughout tissues via exchange of ions and charged molecules through gap junction channels, which themselves are often voltage-gated (Hervé and Derangeon, 2013). This creates a tractable and powerful medium for widespread V_{mem} signaling that has been shown to regulate large scale morphological events in development (Hotary and Robinson, 1992; Jaffe and Nuccitelli, 1977) and regeneration (Jenkins et al., 1996; Levin, 2007). Experimental disruption of endogenous bioelectric patterns has triggered the development of stable morphological abnormalities such as functional ectopic eyes on *Xenopus* flanks (Pai et al., 2012) and healthy two-headed flatworms (Oviedo et al., 2010). Also in *Xenopus*, tumor-like structures induced by oncogene overexpression are characteristically depolarized, but this tumor-like phenotype is rescued with experimental hyperpolarization, despite continued oncogene overexpression (Chernet and Levin, 2013). Together these data show bioelectricity to be an important regulator

of large-scale tissue and organ behaviors and identities, making it a particularly intriguing candidate for stem cell control as opposed to other biophysical influences of differentiation such as osmolarity (Caron et al., 2013), cytoskeletal tension (Ruiz and Chen, 2008), and cell volume (Guo et al., 2017; Lee et al., 2019), which are less associated with such powerful and dynamic signaling. In order to understand and leverage the potential of both bioelectricity and stem cells, it is critical that the interaction between bioelectricity and stem cell differentiation is investigated.

Indeed, there is growing literature on the bioelectric influences over individual cell identity. A cell's resting V_{mem} varies depending on cell type: less specified, more plastic cells like stem cells or cancer cells tend to be more depolarized, while mature cells, particularly excitable cells like myocytes and neurons, tend to be more hyperpolarized (Binggeli and Weinstein, 1986). At the level of the individual cell, V_{mem} also regulates events such as migration, proliferation, and differentiation, the focus of this research project (Blackiston et al., 2009; Sundelacruz et al., 2009). For example, human myoblast differentiation may be dependent on hyperpolarization (Konig et al., 2004; Liu et al., 1998), and timing of V_{mem} fluctuations relative to cell cycle phase may determine ESC differentiation (Ng et al., 2010). Again, this provides a medium through which researchers can manipulate important cell behaviors by modulation of ion gradients, ion channels, and gap junctions. Experimental hyperpolarization accelerates neurogenesis *in vivo* (Vitali et al., 2018), and interventions triggering sustained depolarization of mature neurons and cardiomyocytes can force cell cycle reentry and proliferation, a sort of dedifferentiation that does not occur under standard conditions (Cone and Cone, 1976; Lan et al., 2014).

Here, we focused on mesenchymal stem cells (MSCs). MSCs are a category of adult stem cells that lack a universal definition, but the Society for Cellular Therapy has proposed that they be defined by the criteria that they (i) are plastic-adherent in cell culture, (ii) express cell surface markers *CD105*, *CD73*, and *CD90* while suppressing expression of *CD45*, *CD34*, *CD14* or *CD11b*, *CD79-alpha* or *CD19* and *HLA-DR*, and (iii) can undergo adipogenesis, chondrogenesis, or osteogenesis *in vitro* (Dominici et al., 2006), the chemical signals (Scott et al., 2011; Zhu et al., 2011) and molecular pathways (Komori, 2010; Lefterova et al., 2014) behind which are well characterized.

In addition, MSCs have been isolated for culture from many locations in the human body including bone marrow (Pettinger et al., 1999), peripheral blood (Kadir et al., 2012), and adipose tissue (Wagner et al., 2005). MSCs can also be sourced from the reprogramming of adult somatic cells into induced pluripotent stem cells (iPSCs) (Takahashi et al., 2007) and the subsequent specification of iPSC-derived MSCs (iPSC-MSCs) (Lian et al., 2010). Such accessibility makes MSCs a good tool for stem cell research *in vitro*, and their immunomodulatory features make them exciting candidates for tissue transplantation and regenerative medicine (Figueroa et al., 2012; Stagg, 2006). In addition, there is growing evidence that some disorders such as obesity (Cao, 2011; Louwen et al., 2018), osteoporosis (Kawai et al., 2012; Pino et al., 2012), and aging-related bone loss (Moerman et al., 2004) are at least in part disorders of the balance between MSC adipogenesis and osteogenesis. As a result, MSCs serve not only as a practical stem cell research tool, but an improved understanding of their behavior may directly shape future therapeutics.

The standing literature on the bioelectric influences on MSC differentiation has focused primarily on adipogenesis and osteogenesis. MSC differentiation has been shown to be enhanced

by hyperpolarization and suppressed by depolarization, showing bidirectional V_{mem} sensitivity (Sundelacruz et al., 2008). Furthermore, depolarization of pre-differentiated MSCs does not alter lineage plasticity and allows for chemically-driven changes in lineage choice (Sundelacruz et al., 2013), and this response to depolarization may be driven through a voltage-dependent phosphate signaling pathway in early osteoblasts (Sundelacruz et al., 2019). While this work shows the capacity for V_{mem} to move MSCs forwards or backwards along the spectrum of a given chemically-specified lineage, it is still unclear whether or not V_{mem} can influence individual cell fate choice of MSCs or any other type of stem cell in an environment that is permissive for multiple fate commitment.

These questions have arisen over a period that has seen an explosion in the number of relevant genetically encoded fluorescent reporters of dynamic cell characteristic. Both genetically encoded voltage indicators (GEVIs) (Yang and St. Pierre, 2016; Xu et al., 2017) and genetically encoded transcription reporters allow for real-time measurement of V_{mem} and gene expression, respectively. This provides an advantage over other methods of measuring $V_{mem,}$ such as patch clamp (Kornreich, 2007) and fluorescent voltage sensitive dyes (Adams and Levin, 2012), which are disruptive to normal cell culture conditions. Other methods of measuring gene expression, such as immunostaining and chemical stains require cell fixation and cannot be used for real time observation.

To leverage these recent advances, we first generated a toolbox of transgenic MSCs that can be used to investigate the relationship between V_{mem} and stem cell differentiation. These included the genetically encoded voltage indicators ArcLight (Jin et al., 2012) and Mermaid2 (Tsutsui et al., 2013), as well as the gene expression reporters PPRE-H2B-eGFP (Degrelle et al., 2017) and RUNX2-YFP-H9 (Zou et al., 2015), which indicate expression of the adipogenesis

master regulator peroxisome proliferator-activated receptor gamma (*PPARγ*) (Lefterova et al., 2014) and the osteogenesis master regulator runt-related transcription factor 2 (*RUNX2*) (Komori, 2010), respectively. We also used G-GECO1.2 (Zhao et al., 2011), an indicator of calcium signaling, which is a common downstream transduction mechanism of bioelectric signaling (Catterall, 2011) that has been implicated in development (Slusarski and Pelegri, 2007; Sneyd et al., 1998) and even myoblast differentiation (Konig et al., 2006).

We then sought to address the role of bioelectricity in stem fate commitment. Due to the growing number of known influences on stem cell differentiation and the role of bioelectricity in controlling the identity of biological systems, we hypothesized that bioelectricity is a medium through which various signals are integrated and distributed such that stem cells can make a unified decision to generate a given tissue despite potentially ambiguous signals. To test this hypothesis, we exposed hiPSC-MSCs to a bipotential medium capable of inducing both adipogenesis and osteogenesis while manipulating their V_{mem} with ion channel modulators and found that, as previously reported, hyperpolarization increases total differentiation levels, but also that V_{mem} modulation affects the osteogenesis/adipogenesis ratio. Interestingly, these ratios varied depending on the given ion channel modulator, which may show non-uniform and lineage-specific sensitivity to different hyperpolarization magnitudes, thus creating discrete V_{mem} ranges over which fate choice is biased towards either adipogenesis or osteogenesis.

Following the hypothesis that stem cells communicate bioelectrically to coordinate fate commitments, we were curious to see if modulation of gap junction intercellular communication (GJIC) would affect MSCs when exposed to an ambiguous signal. To test this, we cultured MSCs in an adipogenic/osteogenic bipotential medium supplemented with the gap junction inhibitor 2-aminoethyoxydiphenyl borate (2-APB), which has been shown to block Cx40 and

Cx45 (Bai et al., 2006), both of which are expressed by MSCs (Viliunas et al., 2004) and are voltage-gated (Bukasukas and Verselis, 2004). We found that 2-APB inhibition of GJIC enhanced osteogenesis and had no effect on adipogenesis, and although we didn't explicitly investigate a connection between bioelectricity and the effect of 2-APB in this context, the possibility remains for future exploration.

Taken together, these data provide strong evidence that bioelectric modulation can not only move a stem cell along the path of a given lineage, but that it can also influence *which* lineage that will be. This calls for the future establishment of improved methods to monitor specifically what decision individual stem cells are making, revealing in more detail the bioelectric biases in fate choice and the potential that bioelectric cues can drive differentiation by themselves or force stem cells into non-discrete, mixed fates.

Methods

Molecular biology

ArcLight (Addgene #36856), Mermaid2 (a gift from Dr. Dan Kaufman at UCSD), G-GECO1.2 (Addgene #32446), PPRE-H2B-eGFP (Addgene #84393), and RUNX2-YFP-H9 (a gift from Dr. Tsutsui Hidekazu at RIKEN BRC) were excised with restriction enzymes and ligated into the multiple cloning site of an intermediate pENTR1A plasmid with a CAG promoter. Because PPRE-H2B-eGFP and RUNX2-YFP-H9 contain their own promoters, a peroxisome proliferator response element (PPRE) and the *RUNX2* P1 promoter, respectively, the CAG promoter was removed from the pENTR1A plasmid before construct insertion. The constructs were then transferred into the hyperactive *piggyBac* transposase-based vector

pmhyGENIE-3 with neomycin resistance (Marh et al., 2012) using an LR clonase II (Invitrogen), which was used for transfection and generation of stable cell lines.

Cell culture and differentiation

iPSC-derived mesenchymal stem cells were acquired from STEMCELL technologies (catalog #70922) and the standard growth medium used was MesenPRO RS Medium (ThermoFisher #12746012). For differentiation experiments, cells were seeded into 96-well at 40-60% confluency. Upon reaching approximately 80-90% confluency, the medium was switched to either StemPro Adipogenesis Differentiation Medium (ThermoFisher #A1007001) or StemPro Osteogenesis Differentiation Medium (ThermoFisher #A1007201). The medium was changed every three days for at least 14 days. Passages #3-5 were used for all experiments.

Cell transfection and selection

Only passage #2 cells were used for transfection, which was performed using Invitrogen's Lipofectamine 3000 Transfection Kit. Non-transfected cells were selected against with 1 mg/mL of the antibiotic G418 until all control (mock transfection) cells were dead, and transfected cells were maintained in medium with G418 for one additional expansion passage to ensure selection.

Cell counting with trypan blue

MSCs were dissociated from 6-well plates using TrypLE Select (ThermoFisher) and centrifuged for 5 minutes at 400 x g. MSCs were resuspended in 1 mL, and 100 µL of that suspension was diluted into 400 µL of trypan blue. 10 µL of the MSC + trypan blue dilution was

transferred to each counting chamber of a hemocytometer and counted. The number of cells per mL of original cell suspension = # of cells / square x dilution factor (5) x 10,000.

Alizarin Red S staining and measurement

2 g Alizarin Red S (Sigma-Aldrich) were dissolved in 90 mL distilled water. pH was adjusted to 4.1-4.3 using ammonium hydroxide, and the solution volume was then brought to 100 mL by adding water. Cells were fixed with 10% formalin for 30 minutes at room temperature. The Alizarin Red S solution was filtered using a 0.22 µm filter immediately before adding 100 µL per well to a 96-well plate for 45 minutes at room temperature. A 45-minute incubation period resulted in counterstaining of undifferentiated cells in early characterizations and was adjusted to 30 minutes in quantified experiments to reduce non-specific background. Wells were then washed 4 times with dH_2O and imaged in dPBS. Prior to quantification, wells were again washed 4 times with dH_2O and then incubated in 50 µL 10% acetic acid for 30 minutes with shaking. Cells were scraped off of each well and transferred with the eluent into a 1.7 mL microcentrifuge tube. Tubes were sealed with parafilm, vortexed, heated at 85°C for 10 minutes, cooled on ice for 5 minutes, and centrifuged at 20,000g for 15 minutes. The 50 µL of supernatant from each tube was transferred back into individual wells of a 96-well plate, and 18 µL of 10% ammonium hydroxide was added to each well to neutralize the acetic acid. 50 µL of the resulting solution was transferred to a 96-well plate and the concentration of Alizarin Red S was quantified spectrophotometrically at 405 nm with a microplate reader (SpectraMax M3, Molecular Devices).

Oil Red O staining and measurement

To make the stock solution, 60 mg Oil Red O (Sigma-Aldrich) were dissolved in 20 mL 100% isopropanol. Cells were fixed with 10% formalin for 30 minutes at room temperature. Cells were incubated for 5 minutes with 60% isopropanol at room temperature before staining. Working solution was made by adding 3 parts stock solution to 2 parts dH_2O, and working solution was filtered with a 0.22 µm filter before adding 100 µL per well to a 96-well plate for 45 minutes at room temperature. Wells were then washed 4 times with dH_2O and imaged in dPBS. Before elution, cells were washed 3 times with 60% isopropanol for 5 minutes at room temperature with shaking. Elution was then performed by incubating cells with 100 µL of 100% isopropanol for 5 minutes at room temperature with shaking. 50 µL of the eluent was transferred to a 96-well plate, and the concentration of Oil Red O was quantified spectrophotometrically at 518 nm using a microplate reader (SpectraMax M3, Molecular Devices).

Alizarin Red S and Oil Red O combined staining

For all staining that was ultimately quantified, Alizarin Red S and Oil Red O staining were performed together. All steps from above were followed, but in the following order of major events: Fixation, Oil Red O staining, Alizarin Red S staining, imaging in PBS, an additional 4 washes with dH_2O, Oil Red O elution, Alizarin Red S elution, quantification.

Imaging and image analysis

Unless otherwise noted, images were acquired using the EVOS FL Auto 2 Imaging System (ThermoFisher) with a 20x objective. The intensity and exposure of all fluorescent images were held constant within each experiment. GFP images were acquired using the EVOS

LED Cube, GFP (AMEP4651) and YFP images were acquired using the EVOS LED Cube, YFP (AMEP4654). For GEVI characterization of V_{mem} responses to ion channel-modulators, whole-field mean pixel intensities were retrieved using ImageJ's "Plot Z-axis Profile" option, and raw data was extracted directly from ImageJ. To assess changes in brightness in fluorescent transcription reporters, contrast and brightness were adjusted using ImageJ's auto adjust feature on the image from t =72 hours. The image from t = 8 hours was then adjusted to the same thresholds, so that each within-condition pair of images was processed equally.

Microfluidics

Microfluidics experiments were performed using a microfluidics chip described previously (Dungan et al., 2017), except instead of measuring cell conductivity, the chip and microfluidics system was used to allow fluorescent measurement of MSC-Arclight V_{mem} responses to cell culture media containing bioelectric modulating drugs or molecules. Cells were plated onto matrigel-coated PDMS slides and allowed to attach for at least 24 hours before testing, and test media were heated at 37°C overnight the night before testing to force gases out of solution to prevent bubble formation in the microfluidics system. All drugs or molecules were added to media and mixed gently as to avoid bubbling immediately before testing. A flow rate of 3.4 mL per hour was used.

Statistics

Statistics were performed using Prism v.5 (GraphPad Software, La Jolla, CA, USA). To compare differentiation levels depending on treatment condition, group means were analyzed using a one-way ANOVA followed by a post-hoc Tukey HSD was performed to compare group means. To compare the mean number of cells in wells cultured with or without 2-APB, a

student's t-test was performed. To assess correlation between absorbances of eluted stains at 518 and 405 nm, a linear progression was performed. Tiered significances were reported ($p<0.0332$ (*), 0.0021 (**), 0.0002 (***), 0.0001 (****)).

Results 1: Tool Building

Genetically encoded indicators of voltage and calcium

In order to measure fluctuations in MSC V_{mem}, we generated MSC lines with the bright, slow responsive GEVI ArcLight, for which a 35% change in GFP fluorescence corresponds to an ~100 mV change in V_{mem} (Jin et al., 2012). ArcLight has a linker region that is embedded in the plasma membrane attached to an intracellular GFP that increases its brightness upon hyperpolarization (**Figure 1A**) (Broussard et al., 2014). In MSCs, ArcLight showed good membrane localization (**Figure 1B**), which is critical for GEVI detection of and feedback regarding V_{mem} changes. We also used the CFP-YFP fluorescence resonance energy transfer (FRET) reporter Mermaid2 (Tsutsui et al., 2013), which showed excellent membrane localization (**Sup. Figure 1A**). ArcLight was used to characterize MSC V_{mem} responses to ion channel modulating drugs (**Results 3**), and we attempted to characterize V_{mem} changes during differentiation but encountered technical difficulties. Although Mermaid2 was not used later in this project, the ratiometric nature of its FRET response may enable more precise measurements in the future.

In addition, we created an MSC line with the GFP-based genetically encoded calcium indicator (GECI) G-GECO1.2 (Zhao et al., 2011) (**Sup. Figure 1B**). We did not use this cell line in this project, but its availability enables exploration of calcium signaling as a mechanism in V_{mem} responses during differentiation in the future.

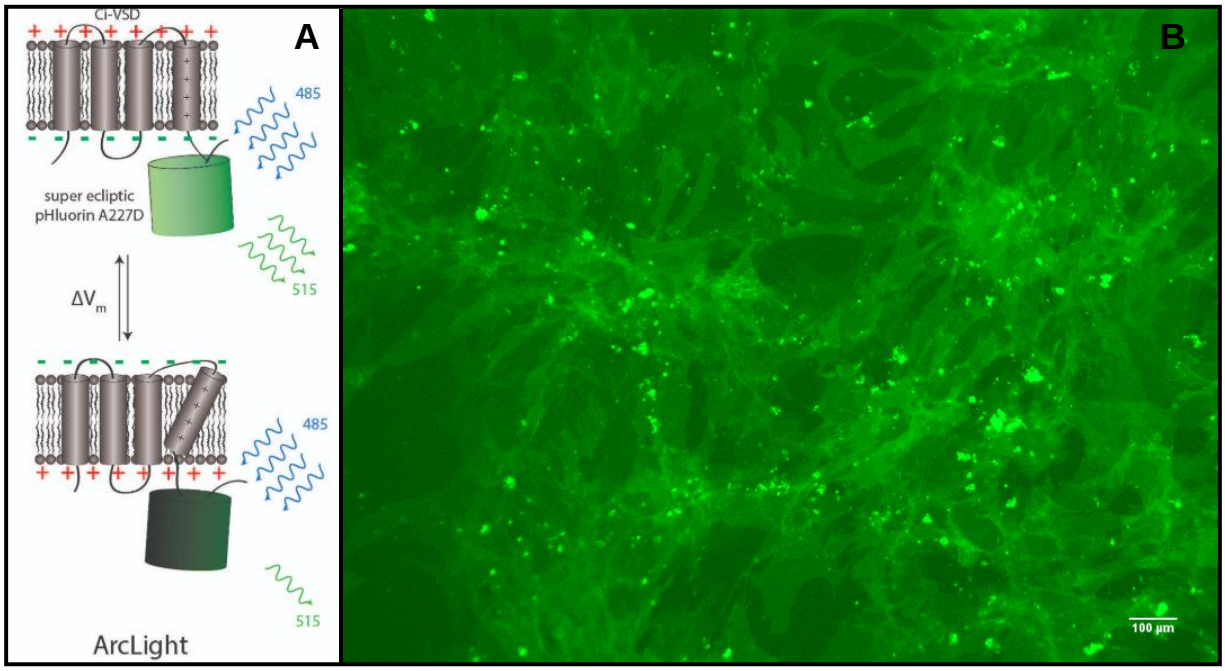

Figure 1. MSC-ArcLights Show Uniform Expression and Good Membrane Localization ArcLight is a membrane bound, voltage sensitive GFP reporter (**A**) (Broussard et al., 2014). MSCs were transfected with ArcLight, and after selection, all cells showed expression of the reporter and good membrane localization (**B**). This picture is of old cells, so bright clumps that can be seen are budding pieces of membrane and not self-assembling ArcLight aggregates. This image was acquired using a Zeiss Axio Observer Z1 with a 10x objective and a GFP filter cube.

By creating these reporters, we successfully enabled the real-time, non-disruptive measurement of V_{mem} and calcium signaling in MSCs that was used in this research project and can be used for other applications in the future.

Genetically encoded indicators of cell lineage-specific gene expression

To monitor real-time changes in the expression of the adipogenesis master regulator PPARγ (Lefterova et al., 2014) and the osteogenesis master regulator RUNX2 (Komori, 2010), we generated MSC lines containing the constructs PPRE-H2B-eGFP (Degrelle et al., 2017) and RUNX2-YFP-H9 (Zou et al., 2015).

We then tested the ability of these transgenic lines to specifically report the initiation of their respective differentiation pathways by culturing them in differentiation media and observing changes in their fluorescence via time lapse over the course of 3 days, with images captured every 8 hours. This 8-hour capture rate was chosen because adipogenic and osteogenic media show significant background fluorescence in the GFP/YFP spectra and a slower capture rate prevents background photobleaching, while still allowing the detection of incremental changes. We expected to see upregulation of *PPARγ* and *RUNX2* expression manifested as increased reporter fluorescence over this relatively short period of differentiation because morphological differences can already be observed after 3 days, and as the "master regulators" of their respective differentiation cascades, *PPARγ* and *RUNX2* upregulation must drive such changes.

As expected, over the 3-day differentiation period we saw an increase in fluorescence from PPRE-H2B-eGFP in adipogenic medium but not in osteogenic or growth medium, indicating proper adipogenic specificity (**Figure 2A-F**). In MSC-RUNX2-YFP-H9s, however, we saw an increase in fluorescence brightness independent of the culture medium, suggesting that it will not be possible to use this particular cell line to identify osteogenic cells (**Figure 2G-L**). Differences in background brightness between groups arose from differences in autofluorescence of each medium, and differences in background fluorescence between groups likely arose from metabolism of the media over the 3-day period.

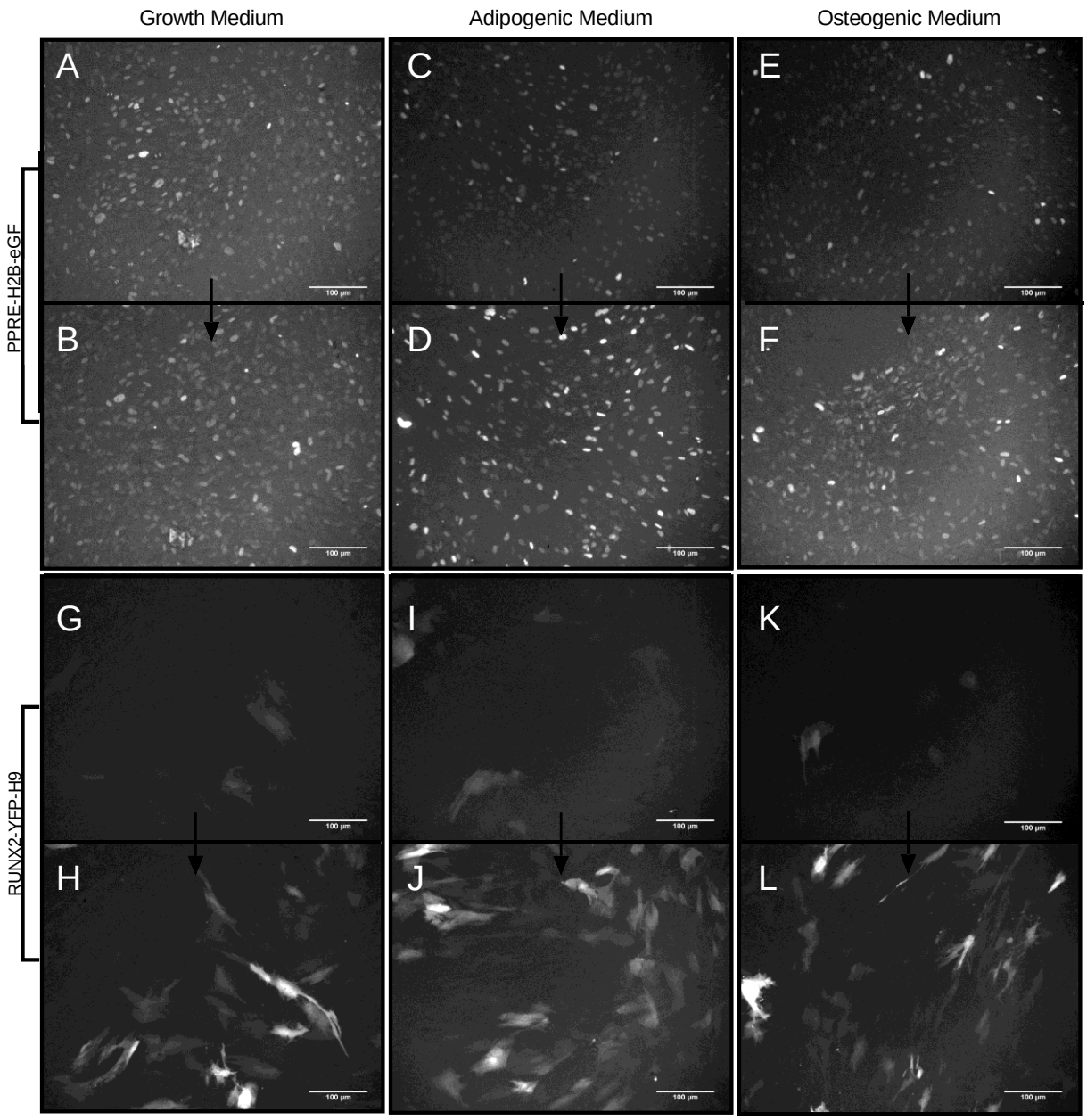

Figure 2. Adipogenic Specificity in PPRE-H2B-eGFP; Lack of Specificity in RUNX2-YFP-H9

MSCs transfected with the adipogenesis reporter PPRE-H2B-eGFP (**A-F**) and the osteogenesis reporter RUNX2-YFP-H9 (**G-L**). MSCs were cultured until 80-90% confluence and then switched into either growth medium, adipogenic medium, or osteogenic medium and observed for 3 days via time lapse. Images were taken every 8 hours to reduce photobleaching, and all images were taken using a YFP filter with the same brightness and exposure. Images from t = 8 hours and t = 72 hours are displayed. To make the reporters visible, contrast and brightness were adjusted using ImageJ's auto adjust feature on the image from t =72 hours. The image from t = 8 hours was then adjusted to the same thresholds, so that each within-condition pair of images was processed equally. Within-condition reporter brightness comparisons show that the brightness of

the PPRE-H2B-eGFP reporter increased only in cells cultured in adipogenic medium (**C-D),** while RUNX2-YFP-H9 brightness increased in all conditions **(G-H, I-J, K-L**).

While additional experiments are still necessary to determine the cause of the lack of specificity that we saw RUNX2-YFP-H9, as a whole these reporters form the foundation of a toolbox that will be used in the future investigation of the relationship between bioelectricity and stem cells.

Results 2: Bipotential Medium Induces Both Adipogenesis and Osteogenesis in Single Populations

In order to confirm that the selected commercially-available kits were able to induce adipogenesis and osteogenesis in our hiPSC-MSCs, we first exposed cells in 24 well-plates to either adipogenic or osteogenic medium. After differentiation periods of various lengths, cells were qualitatively assessed for differentiation by fixation and staining with Alizarin Red S (ARS), which stains calcium deposits produced by osteoblasts, and Oil Red O (ORO), which stains lipid droplets produced by adipocytes (as described in **Methods**). We found that cells cultured in osteogenic medium showed significant ARS staining after 18 days and total monolayer stain saturation after 27 days (**Figures 3B & 3C**), while only mild counterstaining was seen in undifferentiated cells (**Figure 3A**). The ARS protocol was later adjusted (as described in **Methods**) to reduce ARS counterstaining. ORO staining was clear after 18 days (**Figure 3E**), and no staining was visible in undifferentiated cells (**Figure 3D**). These results confirmed both successful differentiation of the MSCs with commercially-available kits and the ability to specifically detect differentiation with the chosen stains.

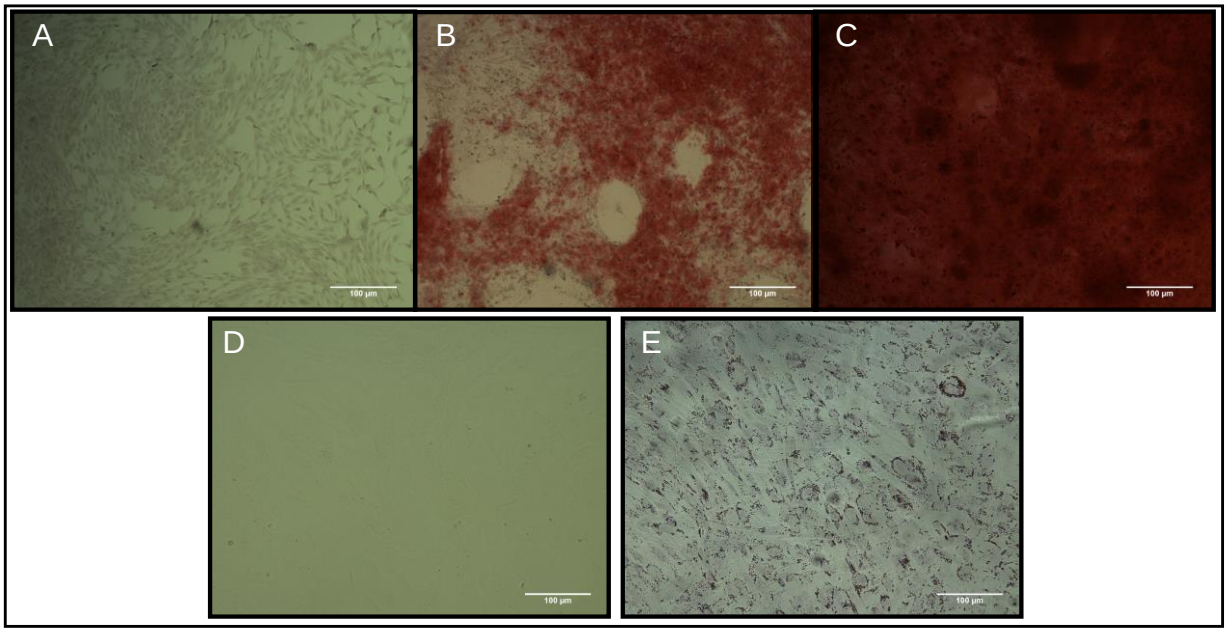

Figure 3. Identification of Adipogenesis and Osteogenesis with ARS and ORO
MSCs were cultured for various time periods in adipogenic, osteogenic, or growth medium. After 18 days in osteogenic medium, significant ARS was observed, and by 27 days, all cells appeared saturated with ARS (**B-C**). Undifferentiated cells that had been cultured in growth medium only showed ARS counterstaining (**A**). MSCs cultured in adipogenic medium showed ORO staining of lipid droplets after 18 days (**E**), and undifferentiated cell from growth medium showed no staining (**D**). NOTE: original pictures of ORO staining were not included due to low image quality, so images from later experiments were used.

We then sought to create a bipotential medium that stochastically induces adipogenesis and osteogenesis like those used in previous studies of the influence of variables like cell volume (Guo et al., 2017) and culture substrate (Han et al., 2014; McBeath et al., 2004) on the stem cell decision making process. We created a bipotential medium by mixing adipogenic and osteogenic media at different ratios and found that osteogenesis was overwhelmingly favored at percentages of osteogenic medium greater than or equal to 25% of total medium volume. At lower concentrations of osteogenic medium, however, significant adipogenesis was preserved and osteogenesis was still detectable (**Figures 4A & 4B**). The discovery of a bipotential medium that

generated appreciable amounts of adipogenesis and osteogenesis allowed for investigation into how V_{mem} biases MSCs to choose one fate or the other.

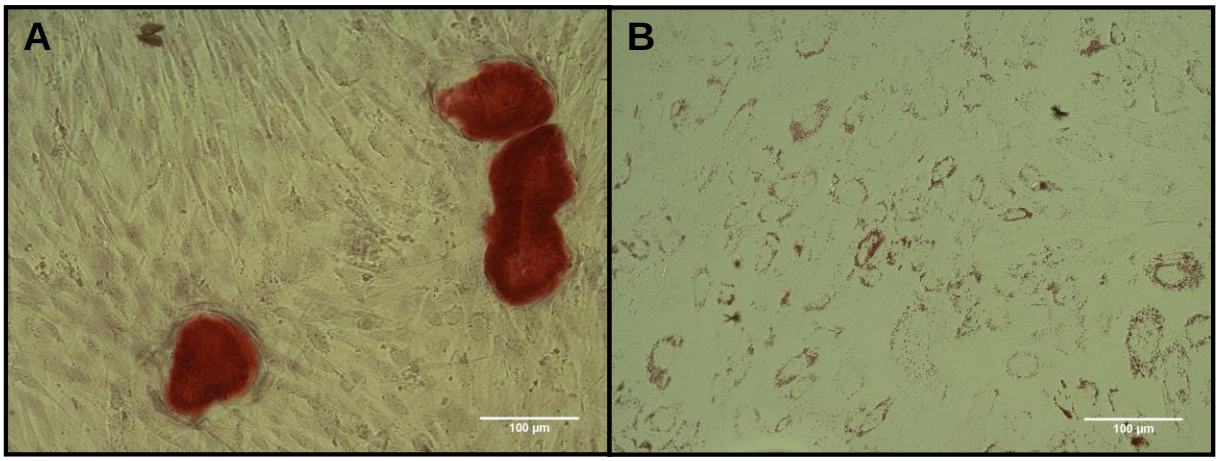

Figure 4. Bipotential medium induced both adipogenesis and osteogenesis
MSCs were cultured in a 95% adipogenic/ 5% osteogenic bipotential medium for 14 days and then stained with either Alizarin Red S or Oil Red O. Positive detection of both osteoblasts (**A**) and adipocytes (**B**) was observed.

Results 3: Bioelectric Modulation of Differentiation in Bipotential Medium

Characterization of V_{mem} responses to ion channel-modulating drugs

After having established the capability to induce a combination of adipogenesis and osteogenesis from bipotential medium, we tested how experimentally manipulating the V_{mem} of MSCs would affect their interpretation of this ambiguous signal. To do this, we first characterized the response of MSCs to the ion channel-modulating drugs diazoxide, pinacidil, and ouabain. Diazoxide and pinacidil are both agonists of the ATP-sensitive potassium channel $K_{ir}6.2$ (Ashcroft and Gribble, 2000) and were thus expected to trigger hyperpolarization via K^+

efflux. Ouabain is inhibitor of the Na^+/K^+-ATPase, which is responsible for maintaining a negative resting V_{mem}, and thus was expected to trigger depolarization.

Using a microfluidics system that allows for uninterrupted live cell imaging while switching between different media, we monitored V_{mem} changes upon drug exposure with MSCs expressing the GEVI ArcLight. Diazoxide, pinacidil, and ouabain all triggered a sustained increase in ArcLight brightness, indicating hyperpolarization, followed by a decrease in brightness upon return to control medium, indicating recovery of a relatively depolarized resting V_{mem} (**Figure 5A-C**). These results for ouabain were unexpected, as ouabain has been shown to induce depolarization in MSCs (Sundelacruz et al., 2008), but not unprecedented (Higashi et al., 1987; Matsumoto et al., 2008). The control showed no such increase in brightness, but a gradual degradation of the signal was seen, most likely due to photobleaching (**Figure 5D**). Similar signal degradation was seen in treatment conditions, so while there appears to be a diminishing effect of the course of each treatment, this may actually be photobleaching of an unchanging state. In all conditions, a brief, large hyperpolarization was seen t = 20 and t = 140, the points at which valve changes were made, and as this was seen in the control, it appears to be an artifact of the valve switch and not a short-term drug effect. When plotted together, all of these patterns can be seen (**Figure 5E**). The relative magnitude of the within-group fluctuations cannot be compared across groups due to differences in baseline brightness that arose from differences in the number and brightness of cells in any given trial.

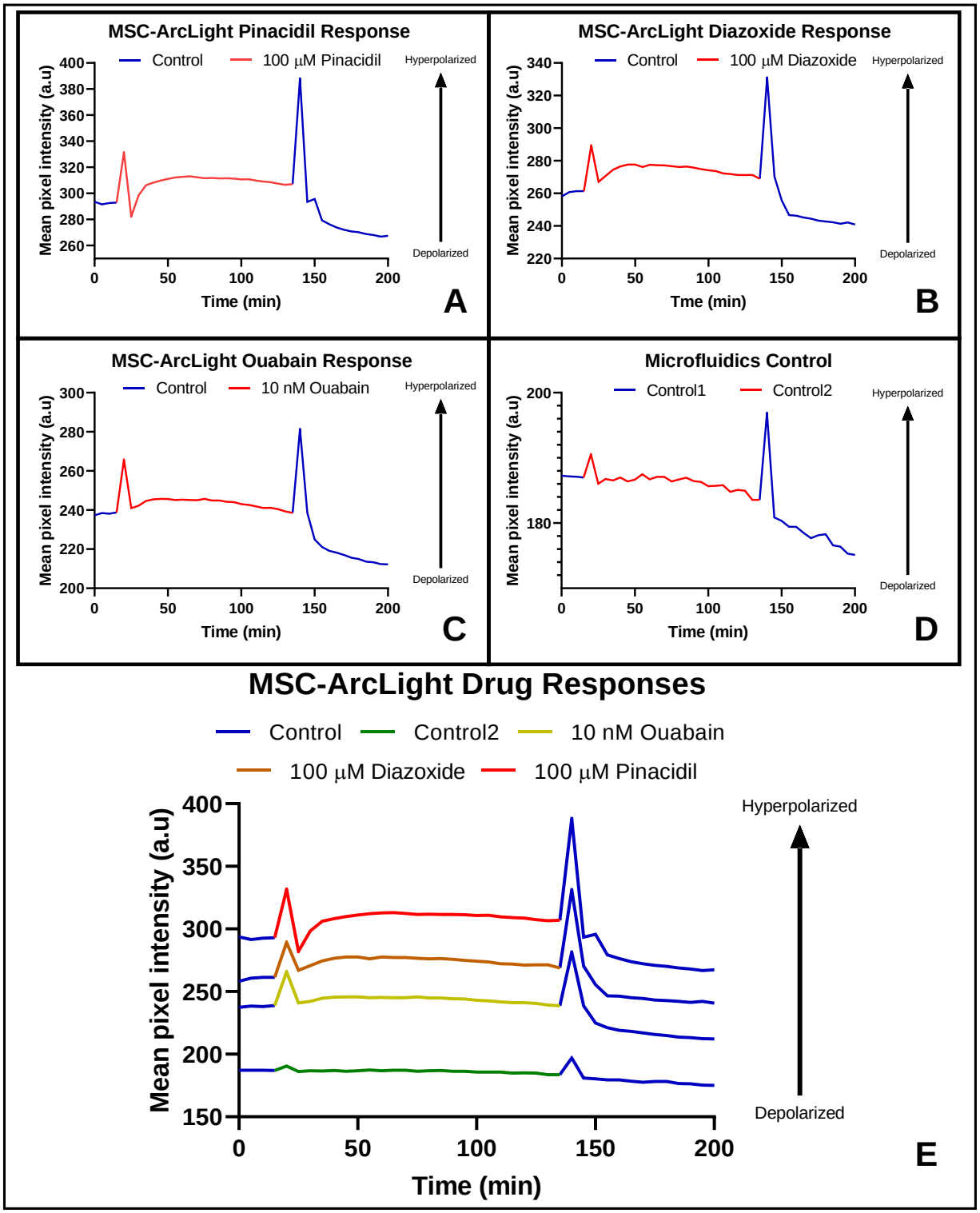

Figure 5. Diazoxide, Pinacidil, and Ouabain Hyperpolarize MSCs
MSC-ArcLights were imaged using a GFP filter every 5 minutes for 200 minutes: 20 minutes growth medium; 120 minutes growth medium + treatment; 60 minutes growth medium. Image intensity, exposure time, and MSC passage # were held constant for all trials, but a new aliquot

of cells was used for each trial. Whole-field average pixel intensity was extracted from ImageJ and plotted. MSC-ArcLights exposed to diazoxide, pinacidil, and ouabain all showed a sustained increase in brightness, indicating hyperpolarization (**A-C**). As a control, growth medium was switched with a separate source of growth medium, which did not result in any sustained changes in V_{mem}, but gradual signal degradation was seen (**D**). When plotted together, all of the patterns can be seen (**E**), but because absolute values varied depending on the number of cells and the baseline brightness of the cells in any given trial, cross-trial comparisons cannot be made.

Hyperpolarizing ion channel modulators alter the ratio of osteogenesis/adipogenesis in bipotential medium

To measure the effect of bioelectric modulation on adipogenic/osteogenic fate commitment, we cultured MSCs in bipotential medium with an osteogenesis/adipogenesis medium ratio of 20/80 supplemented with .1% DMSO (control), 100 μM diazoxide, 100 μM pinacidil, or 10 nM ouabain (**Sup. Figure 2C-F**), all three of which are ion channel modulators that appeared to induce hyperpolarization in these MSCs (**Results 2: Figure 1**). A 100% adipogenic medium condition was also included as a control (**Sup. Figure 2A**), and a 100% osteogenic medium control was attempted but lost due to cell monolayer disruption. A 60 mM hypertonic K^+-gluconate condition was included as well (**Sup. Figure 2B**), which interestingly entirely suppressed osteogenesis (**Figure 6A**). Increased extracellular K^+ is commonly used to induce depolarization, but osmotic stress has been shown to hyperpolarize cells even when caused by hyperosmolar K^+ (Dall'Asta et al., 1993; Gönczi et al., 2007). In addition, hyperosmotic K^+ can alter cell behavior independent of V_{mem} (Erndt-Marino et al., 2017). Because no effect from V_{mem} in this condition could be isolated, these results are not further analyzed here.

All three hyperpolarizing drugs significantly enhanced osteogenesis (**Figure 6A**), while only pinacidil enhanced adipogenesis (**Figure 6B**). In order to compare levels of osteogenesis and adipogenesis, ARS and ORO absorbance readings were normalized relative to blank ARS

and ORO solvents, water and isopropanol. Using these normalized values, we saw that diazoxide and ouabain generated significantly different osteogenesis/adipogenesis ratios compared to pinacidil and the bipotential medium wit DMSO (**Figure 6C**). Total levels of differentiation were determined by adding normalized values of adipogenesis and osteogenesis and were also significantly increased in all three hyperpolarizing conditions (**Figure 6C**), but no trend was seen between total levels of differentiation and cell type ratios. Therefore, we conclude that hyperpolarization alters fate choice in a manner that is dependent on the nature of the hyperpolarization and independent of total levels of differentiation.

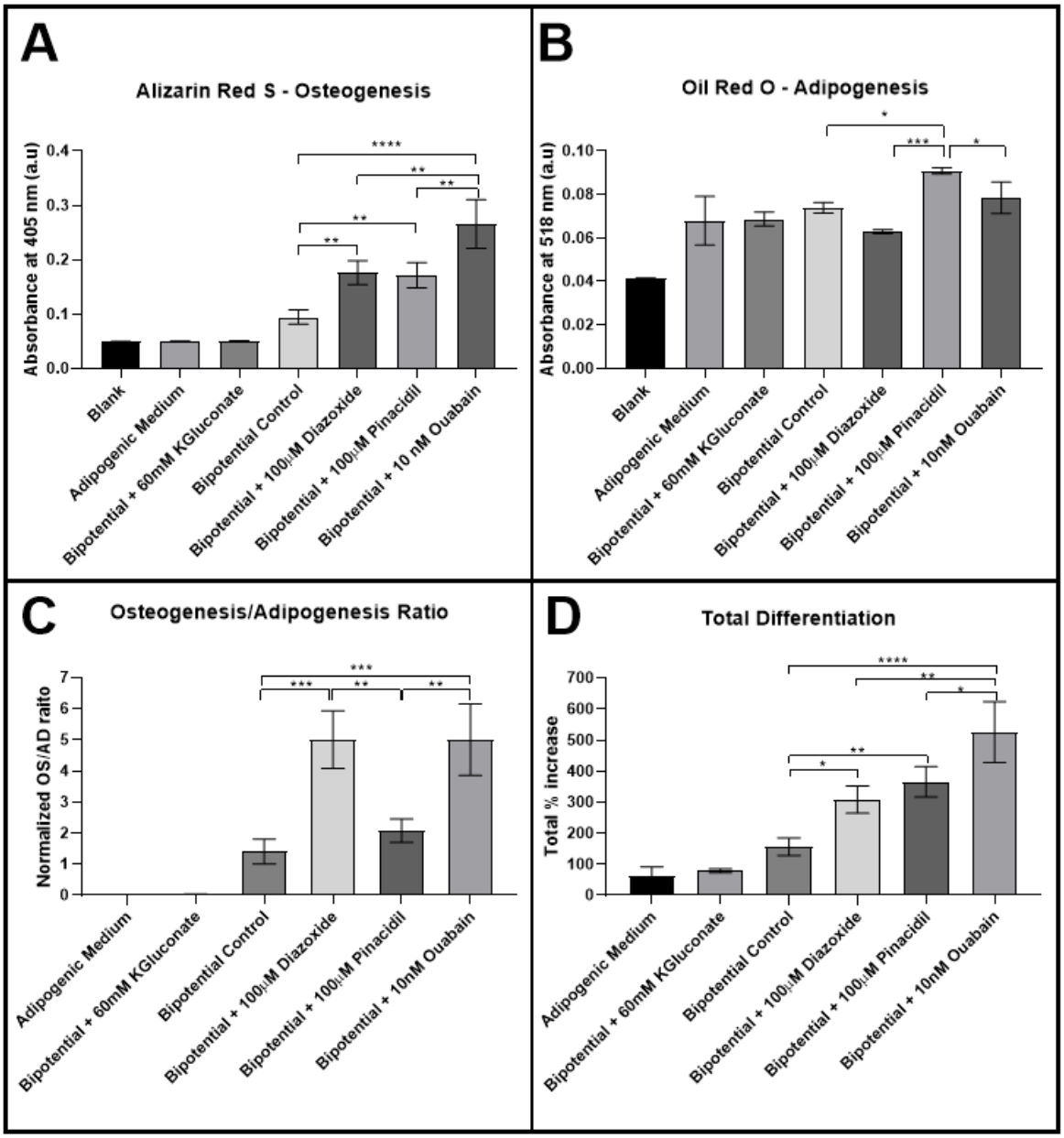

Figure 6. Hyperpolarizing Treatments Alter the Osteogenesis/Adipogenesis Ratio
After differentiation for 18 days in bipotential medium consisting of 80% osteogenic and 20% adipogenic media that was supplemented with .1% DMSO (bipotential control), 100 μM diazoxide, 100 μM pinacidil, or 10 nM ouabain, MSCs were stained with Alizarin Red S (osteogenesis) and Oil Red O (adipogenesis) and then quantified (as described in **Methods**). A one-way ANOVA with a with a post-hoc Tukey HSD was performed to compare group means (n=3, $p<0.0332$ (*), 0.0021 (**), 0.0002 (***), 0.0001 (****)). All three hyperpolarizing conditions showed enhanced osteogenesis (**A**), while only bipotential medium + pinacidil enhanced adipogenesis (**B**). In order to compare levels of osteogenesis and adipogenesis, the data was normalized relative to "blank" water and isopropanol absorbance levels, the respective solvents for Alizarin Red S and Oil Red O. This showed that the hyperpolarizing conditions also

modified the osteogenesis/adipogenesis ratio (**C**) in a manner independent of total levels of differentiation (**D**).

Gap junction inhibition via 2-APB augments osteogenesis in bipotential medium

Following the hypothesis that V_{mem} plays a role in the determination of which lineage a population of cells will favor in the presence of an ambiguous differentiation signal, we examined the importance of gap junction intercellular communication (GJIC) in mediating cell lineage choice. To do this, we cultured MSCs in bipotential media with adipogenic/osteogenic ratios of 100/0, 90/10, 85/15, and 80/20 either with or without the gap junction inhibitor 2-APB at 25 μM.

We found that, independent of the composition of the bipotential medium, 2-APB had no effect on adipogenesis (**Figure 7A)**; however, 2-APB increased osteogenesis, particularly at higher concentrations of osteogenic medium (**Figure 7B**). Aside from the 100% adipogenic controls (**Figure 7E, I**), at every point along the progression of increasingly osteogenic media, cells cultured in 2-APB showed darker Alizarin Red S staining (**Figure 7F-H**) when compared to those cultured without 2-APB (**Figure 7J-L**).

We were then curious if this apparent increase in osteogenesis could be the result of 2-APB reducing contact inhibition in treated cells, leading to a greater number of cells per well. To test this, MSCs were plated at equal densities in 6-well plates and cultured in growth medium + .05% DMSO or growth medium + 25 μM 2-APB until they were 3 days past-confluent. Cells from each condition were then counted. A student's t-test was performed to compare group means, and no significant difference was found between cells cultured with or without 2-APB ($n = 3$, $p = .46$). Thus, we concluded that 2-APB enhances MSC osteogenesis in bipotential medium and does not simply allow for higher post-confluence proliferation rates.

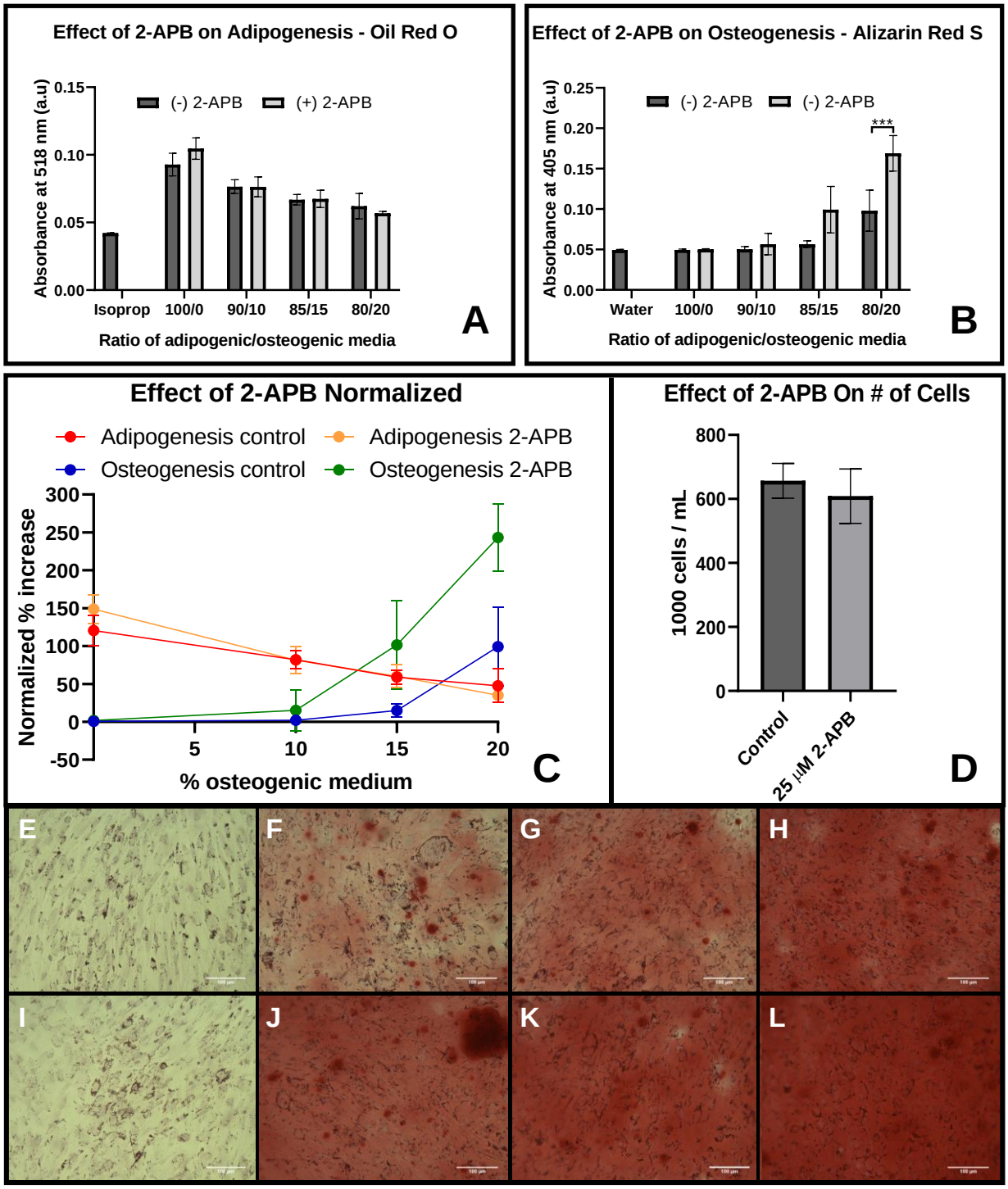

Figure 7. 2-APB Enhances Osteogenesis but not Adipogenesis in Bipotential Medium
MSCs were cultured for 22 days in bipotential media at a range of adipogenic/osteogenic composition ratios with or without the gap junction inhibitor 2-APB (25 µM). Adipogenesis and osteogenesis where then measured with Oil Red O (adipogenesis) and Alizarin Red S

(osteogenesis) (as described in **Methods**). A one-way ANOVA with a with a post-hoc Tukey HSD was performed to compare group means (n = 3, p<0.0332 (*), 0.0021 (**), 0.0002 (***), 0.0001 (****)). Significances between (+) 2-APB and (-) 2-APB conditions with the same medium composition are displayed. 2-APB had no effect on adipogenesis (**A**) but enhanced osteogenesis, particularly at higher concentrations of osteogenic medium (**B**). These trends were normalized relative to the absorbances of each stain's respective solvents, and adipogenic and osteogenic trends were plotted together (**C**). At all points along the progressively osteogenic media, MSCs cultured with 2-APB showed stronger ARS staining (**F-H vs J-L**), while 2-APB did not appear to influence ORO staining (**E & I**). Later, a cell count was performed and a student's t-test showed no significant difference in the number of cells in wells cultured with or without 2-APB (n=3, p =.46) (**D**).

Discussion

Genetically encoded reporters

Here, we generated MSC lines containing the GEVIs ArcLight and Mermaid2, the GECI G-GECO1.2, and the gene expression reporters PPRE-H2B-eGFP (adipogenesis) and RUNX2-YFP-H9 (osteogenesis). We generated MSC lines with these reporters because they provide nondisruptive means to make long-term observations *within a single cell population* with high temporal resolution, potentially enabling the detection of patterns that would have been inaccessible to the measurements at distant time points across different cell populations made previously (Sundelacruz et al., 2008). This is particularly important in a slow and sensitive process like differentiation.

ArcLight was used to characterize V_{mem} responses to ion channel-modulating drugs, while Mermaid2 and G-GECO1.2 were not used after cell line generation. This was due to the time restrictions of ensuring proper function and because we did not study calcium signaling here, but they are now available for use in future projects.

PPRE-H2B-eGFP and RUNX2-YFP-H9 were observed via time lapse for a 3-day differentiation period. The main limitation behind our characterization of PPRE-H2B-eGFP and RUNX2-YFP-H9 was that we did not measure their activity quantitatively. This was because we

could not use whole-field mean pixel intensity as we did with our short-term V_{mem} characterizations. Over a 3-day period there is significant proliferation, which fills up the background and thus increases mean pixel intensity without an increase in signal from individual cells. In addition, there appeared to be changes in the autofluorescence from some of the media, which we believe to be due to the metabolism of the media over the 3-day period. To compare reporter brightness before and after culture in the various media, we used ImageJ's auto contrast/brightness adjust feature on the second of the two images from each group and matched the thresholding of that image to the first. This was intended to process each pair of images equally so that a comparison could be made visually. This is ultimately subjective, by no means a robust or complete method, and should be replaced in the future with quantitative methods.

Using this method, however, PPRE-H2B-eGFP showed an increase in brightness only in adipogenic medium, indicating proper function. Because this cell line was not clonally pure, there were visible differences in baseline expression levels as well as uneven increases in brightness over the 3-day observation period. For more accurate measurements in the future, uniformity can be attained by generating a clonally pure cell line, and stronger signals might be observed over a longer differentiation period.

RUNX2-YFP-H9 showed increased brightness over the 3-day period independently of its culture medium, indicating either non-specific promoter function of the reporter or spontaneous osteogenesis in the absence of osteogenic chemical inducers. While MSCs have shown spontaneous upregulation of RUNX2 without specific osteogenic signals (Sonomoto et al., 2016), this was not until day 7 of culture, and we have observed low levels of spontaneous differentiation in these MSCs. As a result, it is unlikely that this increase in reporter fluorescence is indicative of actual *RUNX2* gene expression. When all images were examined, this apparent

increase in fluorescence did not appear to come from the proliferation of a few unusually bright cells, and with the low rate of image capture, it is most likely not a false positive from differential medium/fluorophore photobleaching rates. RUNX2-YFP-H9 was originally tested in ESCs (Zou et al., 2015), so future troubleshooting of this construct should involve testing in other stem cell populations and beginning with clonally pure populations that show low basal reporter expression levels.

V_{mem} measurement precision and use of microfluidics

ArcLight was used for characterization of MSC V_{mem} responses to the ion channel modulators diazoxide, pinacidil, and ouabain. We chose ArcLight for its bright responses (~35% change in brightness per 100mV) and its familiarity within our lab. One of the limitations of ArcLight that may be a concern is the notorious sensitivity of GFP to changes in pH (Campbell and Choy, 2001). ArcLight's GFP is also a pHluorin, which is a variation of GFP that is designed to be particularly pH sensitive (Miesenbock et al., 1998). Still, this most likely did not impact our drug response characterizations, which were performed under constant perfusion and thus a constant source of fresh medium. For future long-term V_{mem} characterizations of differentiation, however, in which the medium cannot be changed, this factor should be considered. In those cases, Mermaid2 might serve as a superior alternative, although its CFP-YFP fluorophores are still somewhat pH sensitive (Betolngar et al., 2015)

Using a GEVI in combination with a microfluidics system that allows for uninterrupted imaging with medium switches provided the advantages of studying MSC V_{mem} responses within a single population of cells in close-to-standard culture conditions. When doing this, an average cellular response emerges from the mean pixel intensity of the entire image, whereas other

methods such as patch clamping and fluorescent dyes are more invasive and often require the collections of larger sample sizes to compare across conditions because within-cell comparisons between conditions cannot be made accurately. It also allows for potentially much longer observation periods with no additional stress to the cells, unlike patch clamping and fluorescent dyes. The limitation of this method, however, is that within-trial comparisons are the only comparisons that can be made because there is nothing that anchors the fluorescence intensity to known V_{mem} values, especially when performing whole-field imaging with no background subtraction. Variations in baseline brightness occurred due to variations in the number of cells and the brightness of cells, which were not clonally pure, in any given trial. As a result, the only takeaway that we could make from our measurements was the impact of the treatment on the direction of V_{mem} change, with no means to precisely compare the absolute magnitudes of those changes.

In addition, the use of a microfluidics system also introduces some logistical challenges. For example, a small hyperpolarization was observed at the first medium switch from control to treatment, and then a large hyperpolarization was observed when switching back to control medium after an hour. Some stress responses trigger hyperpolarization (Gönczi et al., 2007) and this hyperpolarization is most likely a stress response to a brief influx of cold medium. Although the tubes that hold the different media and the imaging chamber that holds the cells are heated, the tubing that connects the two are not, and these tubes are always filled so that the medium is directly interfaced with the microfluidics chip and no bubbles are pushed across the cells when valve switches are made. As a result, the longer the interval between valve switches, the longer the media in the tubes have to cool and the more stressful it is for the cells upon switches. Not

only does this stress the cells, but it also obscures any interesting signal that might be otherwise detectable within the first several minutes of treatment exposure.

Implications of hyperpolarization-altered fate choice ratios

In this experiment, MSC V_{mem} responses to the ion channel-modulating drugs diazoxide, pinacidil, and ouabain were measured with the GEVI ArcLight, showing hyperpolarization in all three cases. MSCs were then cultured in an osteogenic/adipogenic bipotential medium with one of the aforementioned drugs, and levels of fate choice were quantified using the lineage-specific stains Oil Red O and Alizarin Red S, respectively. We demonstrated that hyperpolarization alters MSC fate choice, as measured by the normalized ratios of osteogenesis/adipogenesis, in a manner that is dependent on the nature of the hyperpolarization and independent of total levels of differentiation, which were increased in all hyperpolarizing conditions. These results corroborate earlier findings that hyperpolarization enhances osteogenesis (Bhavar et al., 2019; Sundelacruz et al., 2008).

A particularly interesting difference between the results here and those from Sundelacruz et al. is the previous finding that ouabain induced depolarization and reduce osteogenesis in bone marrow-derived MSCs, compared to our finding that ouabain hyperpolarized and increased osteogenesis in iPSC-MSCs. These different responses may be a result of differences in characteristics between different MSC donors (Assoni et al., 2017) or source tissues (Wegmeyer et al., 2013). Regardless, the synthesis of these results shows that the impact that ouabain makes on differentiation is strictly a product of its effect on MSC V_{mem} as opposed to an independent artifact of its activity. In addition, our results also indicate that adipogenesis may be enhanced by

hyperpolarization, an interaction about which neither a positive nor null result was explicitly reported by Sundelacruz et al.

With regard to cell fate choice, the possibility that hyperpolarization may enhance both adipogenesis and osteogenesis is interesting because it is unlike other biophysical factors that are known to alter fate choice like cell volume (Guo et al., 2017) and substrate (Han et al., 2014; McBeath et al., 2004), which bias MSC fate choice in opposite directions; one state favors adipogenesis and disfavors osteogenesis, while the other state favors osteogenesis and disfavors adipogenesis. In combination with the previous findings from Sundelacruz et al. that depolarization suppresses both adipogenesis and osteogenesis, this would show matching bi-directional sensitivity; hyperpolarization favors both adipogenesis and osteogenesis, while depolarization disfavors both adipogenesis and osteogenesis. Even though signals that affect each lineage in opposite directions seem like better candidates for the influence of individual cell fate choice, all that is required to bias fate choice is differential favoring. This variation in the adipogenesis/osteogenesis ratio across all three hyperpolarizing conditions suggests that the effects of hyperpolarization on adipogenesis and osteogenesis are unidirectional (favorable), but the extent to which each lineage is favored may be magnitude-sensitive and lineage-specific, creating discrete ranges over which one fate is primarily favored.

Testing this hypothesis would require much more precise measurement of V_{mem} and differentiation levels. Unlike the V_{mem} measurements here that were restricted to within-trial comparisons, absolute quantifications would be necessary to reveal differences in hyperpolarization magnitude. For measurement of differentiation, the methods that we used can only detect the amount of each stain per well. These amounts are determined by the total number of cells per well, the percentage of cells that choose a certain lineage, and the extent to which

individual cells express lineage markers. Therefore, the measured values do not account for differences in cell density in each well and how strong a signal is produced by each cell, both of which may vary with treatments. The primary measure of interest when studying fate choice is only the percentage of cells that chose a given lineage, and refining our methods to achieve this should be a priority going forward.

Inhibition of GJIC enhances osteogenesis in bipotential medium

2-APB is known to inhibit voltage-gated gap junctions expressed in MSCs (Bai et al., 2006; Viliunas et al., 2004), and we showed that 2-APB inhibition of gap junction intercellular communication (GJIC) in bipotential medium enhanced osteogenesis and had no impact on adipogenesis. Knockdown of GJIC through some connexins has been shown to suppress contact inhibition of proliferation (Ruch et al., 1995), so we were curious whether or not the increased osteogenesis levels were actually just due to an increased number of cells. After a cell count, however, this did not appear to be the case, indicating that 2-APB, does, indeed, enhance osteogenesis.

We originally pursued this idea because gap junctions allow for transmission of bioelectric signals (Nielsen et al., 2012; Pereda et al., 2012), and if there is truth to the hypothesis that stem cell populations integrate various signals and then bioelectrically coordinate fate choice to make a unified decision, then perhaps inhibition of GJIC would result in a more dispersed spatial distribution of fate choices. However, even without inhibition of GJIC, the bipotential paradigm explored here does not result in coordinated clusters of one fate or another. Still, it is possible that is the case because cells cultured in 2D cannot form complex networks like those that exist *in vivo* and that spatial patterns of coordinated differentiation may arise when similar

experiments are performed in 3D culture. In the paradigm used here, however, this suggests that study of bioelectric fate choice biases is best focused at the level of individual cells as opposed to contiguous cell groups, which don't appear to act in a coordinated manner.

As it pertains to the level of individual cells, because we did not study the effect of 2-APB on MSC V_{mem} when cells were isolated or coupled, these findings cannot necessarily be tied to bioelectricity. Still, the observation of enhanced osteogenesis adds to the current literature on gap junction regulation of differentiation. In mice, GJIC supports hematopoiesis via stromal cell-stem cell coupling (Cancelas et al., 2000; Montecino-Rodriguez and Dorshkind, 2001). However, intra-stem cell GJIC is required for the maintenance of potency and prevention of differentiation in embryonic stem cells (Todorova et al., 2007). Also, murine neural progenitor cells are gap junction-coupled to one another and lose this coupling in two of their three differentiation pathways (Duval et al., 2002). These examples show that the impact of GJIC on differentiation is dependent on the cell type with which the stem cell is coupled. Therefore, if adipocyte-osteoblast or adipocyte-MSC coupling inhibits osteogenesis, then the inhibition of this coupling would result in an increase in osteogenesis relative only to other MSCs and osteoblasts that are co-cultured with adipocytes. As a result, this phenomenon in MSCs should be studied more closely in a 100% osteogenic condition to determine if osteogenesis augmentation from 2-APB occurs universally or only in a bipotential paradigm. In addition, the use of other gap junction inhibitors that target different connexins will be important in determining which connexins are responsible for this phenomenon.

Discussion of a potential confound from sequential elution of ORO and ARS stains

Due to resource restrictions at the time of the experiment, there was not enough medium to culture a sufficient sample size of cells unless osteogenesis and adipogenesis were measured in the same wells using ORO (adipogenesis) and ARS (osteogenesis) together. First ORO was applied, then ARS was applied, then ORO was eluted in 100% isopropanol, and finally ARS was eluted in 10% acetic acid. Although ORO and ARS have absorbance maxima of 518 nm and 405 nm, respectively, there is overlap between their absorbance spectra, which raises concerns of cross-contamination. It was visible that the ORO elution in isopropanol did not leave any ORO behind (**Sup. Figure 2G**), so there is little concern of ORO contaminating the subsequent ARS eluent and measurement. However, despite ARS being insoluble in isopropanol and 8 wash steps (as described in **Methods**) before ORO elution, it is possible that residual ARS was already in solution and contaminated the ORO eluent.

The potential consequence of such contamination was assessed by measuring and plotting standard absorbance curves of ARS and ORO at both 405 and 518 nm (**Sup. Figure 3A-B**). These plots were used to test the hypothetical scenario: During processing of the bipotential medium control condition, what if half of the ARS was eluted with isopropanol during the ORO elution, and the other half is what remained and was later eluted and measured as the final ARS value? Calculations show that, in this scenario, the ARS contamination in the ORO elution would have accounted for 76% of the ORO signal. This scenario vastly overestimates any realistic or mathematically possible amount of ARS contamination but shows that, if there were cross-contamination, the overlapping absorbance spectra or ORO and ARS are such that it would make a significant impact.

When plotted out by condition, however, there is no correlation between ARS and ORO levels between wells from each group (**Sup. Figure 3C**), which is a correlation that might be expected if leakage of high ARS levels contaminated ORO readings. Still, this potential confound may explain why the bipotential medium + ouabain condition, which showed the highest ARS readings, generated relatively high ORO readings as well despite the appearance of very little ORO staining (**Sup. Figure 2F**). In addition, the ouabain group showed the largest within-group correlation between ARS levels and ORO measurements, although it was still statistically non-significant. Overall, the osteogenesis readings were most likely unaffected, but this is a confounder worth keeping in mind and addressing in the future when interpreting adipogenesis results. It should also be noted that a worst-case scenario from this confounder does not detract from the finding that V_{mem} influences stem cell interpretation of ambiguous signals. For example, ouabain induced an increased osteogenesis/adipogenesis ratio, but if adipogenesis amounts were overestimated due to cross-contamination of high ARS levels, then the real osteogenesis/adipogenesis ratio was even more extreme.

Future Directions

Future investigation into the role of bioelectricity in stem cell fate choice should begin with more precise measurement and control of V_{mem}. It is imperative that the variable adipogenesis/osteogenesis ratios that we observed can be mapped onto V_{mem} distributions to confirm that the variable results that were seen are a product of variable bioelectric profiles and not just the drugs used. These absolute value quantifications can be obtained via patch clamp intracellular recordings or a combination of patch clamp and well-characterized fluorescent V_{mem} reporter dyes like $DiBAC(4)_3$, for which a 1% change in fluorescence corresponds to ~1 mV

change in V_{mem} (Erdogan et al., 2005). To increase precision and variation in the source of V_{mem} modulation, extracellular ion concentrations can be manipulated to change their equilibrium potential as modeled by the Nernst equation. This would also be a secure method of depolarization, which we were unable to induce with ouabain.

Another exciting avenue for V_{mem} manipulation is the rapidly growing field of optogenetics (Mattis et al., 2011). Many light-activated ion channels have been designed to induce rapid, short-lasting V_{mem} spikes like those seen in a neuron's action potential, but there have also been developments of more slowly acting optogenetic actuators that may allow for long term modulation of resting V_{mem} (Berndt et al., 2015; Yizhar et al., 2011). Control of stem cell differentiation would be a novel use of optogenetics and open up new worlds of exploration under the umbrella of bioelectricity, such as the effects of temporal V_{mem} fluctuations on stem cell behavior.

Just as precision in the measurement of V_{mem} is essential to future work, precision in definition and measurement of stem cell fate choice levels is necessary. While it is encouraging to see different adipogenesis/osteogenesis ratios, going forward it is important to isolate the percent of cells choosing a given lineage from the "amounts" of each lineage that we are currently measuring. This can be accomplished by shifting to a sparse differentiation cell counting paradigm, which allows for the identification of individual cell fates by probing MSCs for lineage markers, followed by a count of the number of individual cells that have committed to each fate. Such a technique has already been used for counting MSC osteogenesis ratios (Guo et al., 2017), but we will need to ensure that normal differentiation occurs when MSCs are sparsely plated because degree of confluence is known to affect MSC differentiation (Faten and Zaki, 2017). If this strategy is effective, it would not just provide precision, but also reveal what

percentage of cells are not differentiated and how various bioelectric modulations affect the penetrance of chemical differentiation inducers. Furthermore, it opens up the possibility of the incidental detection of bioelectrically modulated stem cells that have entered a non-discrete state between or characteristic of multiple fates, which has not been seen under normal conditions.

While there are many possible experiments that could be done in the future, such as time-lapse characterizations of V_{mem} change during differentiation using GEVIs or tripotential MSC experiments involving chondrogenesis, perhaps the most simple and exciting one would be the induction of differentiation in MSCs via bioelectric modulation in the absence of chemical inducers. This line of work would be largely dependent on the level of spontaneous differentiation that normally occurs in the population. Bone marrow-derived MSCs show significant spontaneous differentiation during long culture periods (Sonomoto et al., 2016), but we have not yet seen spontaneous differentiation in iPSC-MSCs. Further characterization of spontaneous differentiation in these cells is necessary, but if they show low rates of spontaneous differentiation then iPSC-MSCs would provide an exciting opportunity to study purely bioelectrically driven differentiation.

The work done here shows that there is promise in the under-investigated bioelectric control of stem cell fate choice and that there is an abundance of exciting directions for future work. Modern understandings of the complexity that underlies biological processes have revealed just a few of the many amazing mechanisms that produce all biological phenomena, and we are only scratching the surface of the many secrets that are likely entangled in the interaction between bioelectricity and stem cells.

Supplementary Figures

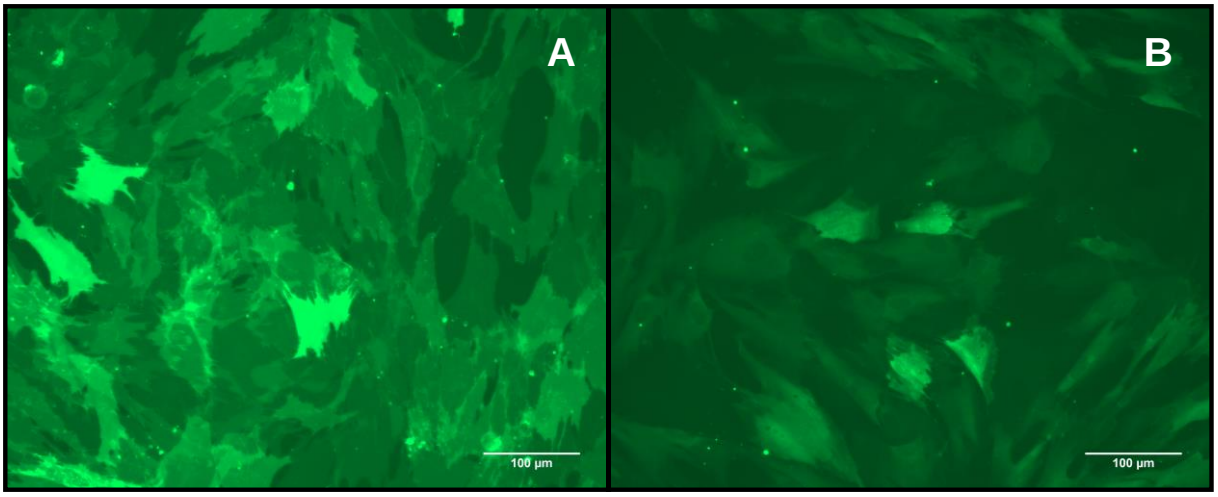

Supplementary Figure 1. Mermaid2 and G-GECO1.2 Show Good Membrane Localization
MSCs were transfected with the fluorescent V_{mem} reporter Mermaid2 (**A**) as well as the calcium reporter G-GECO1.2 (**B**). These transgenic cell lines show expression in all cells and good membrane localization. Image intensity and exposure time varied between images. Images were acquired using a Zeiss Axio Observer Z1 with a 20x objective and a GFP filter cube.

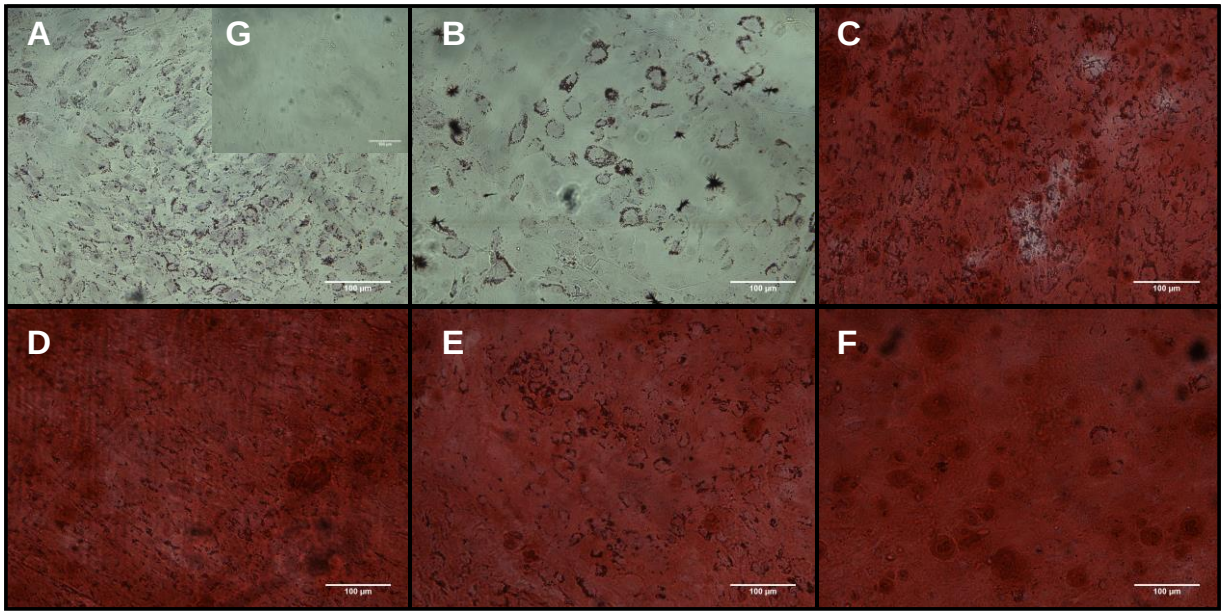

Supplementary Figure 2. Alizarin Red S and Oil Red O Staining of MSCs Cultured in Bipotential Medium with Ion Channel-Modulators

MSCs were cultured for 22 days in 100% adipogenic medium (**A**) or a bipotential medium supplemented with 60 mM K-gluconate (**B**), DMSO (control) (**C**), 100 µM diazoxide (**D**), 100 µM pinacidil (**E**), or 10 nM ouabain (**F**). MSCs were first stained with ORO, and then ARS. There was then full elution of ORO using 100% isopropanol (**G**), followed by elution of ARS with 10% acetic acid.

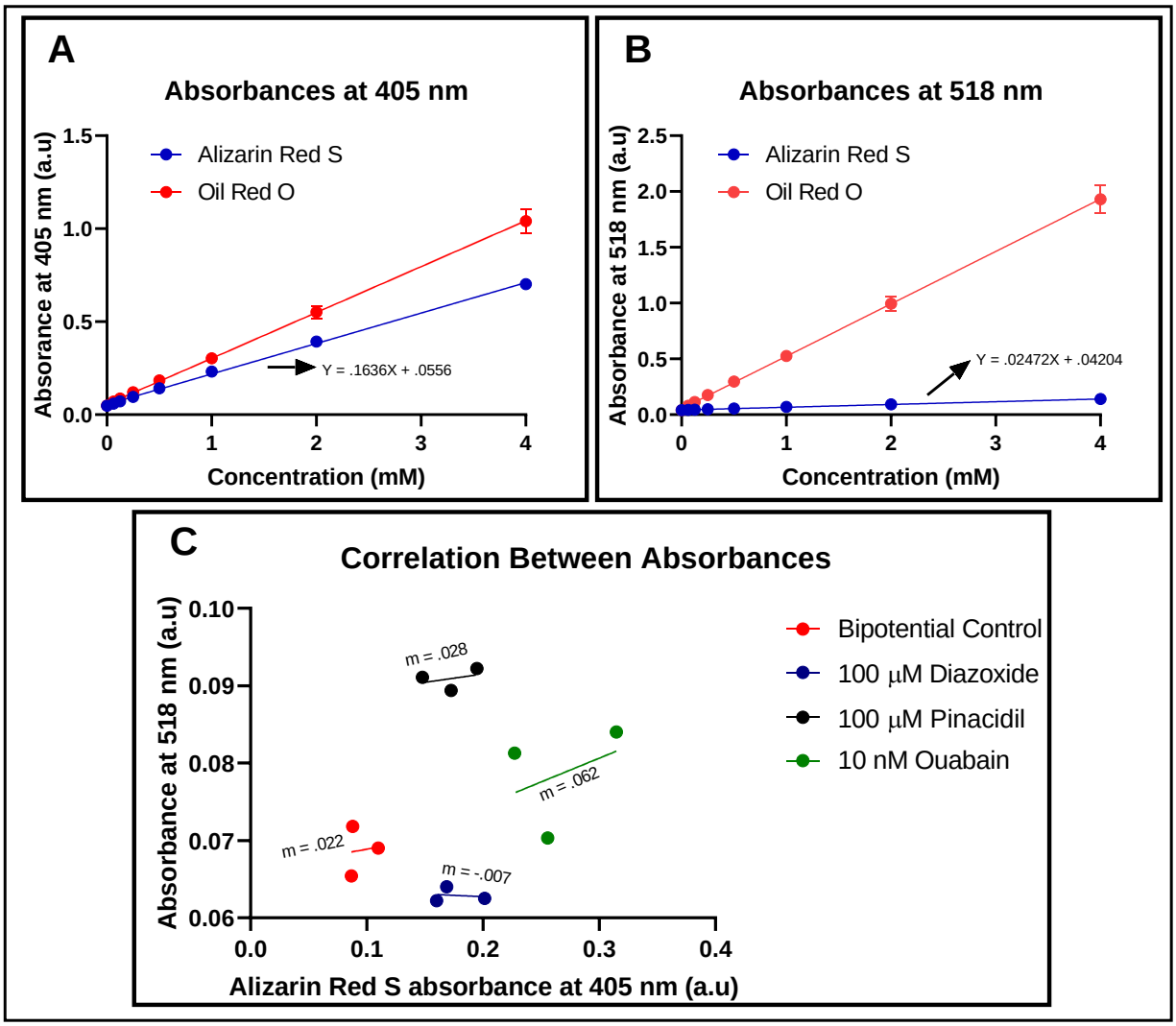

Supplementary Figure 3. Assessment of Potential ARS Contamination of ORO Eluent Standard curves were measured and plotted for Alizarin Red S (ARS) and Oil Red O (ORO) (**A-B**) in order to calculate the potential impact of ARS contamination in the ORO eluent when measured spectrophotometrically at 518 nm. Using the average bipotential control reading at 405 nm of 0.0948 and the equation derived from the ARS standard curve at 405 nm (Y = 0.1636X + 0.0556), it is estimated the average concentration of ARS eluted from this condition was 240 mM. When that concentration is plugged into the equation for ARS absorbance at 518 nm (Y = 0.02472X + 0.04204), it yields a cross-over absorbance of 0.048 a.u, which represents 76% of the bipotential control reading for ORO. The measured absorbance at 518 nm, which was intended to represent only the ORO concentration in the eluent, was then plotted as a function of the absorbance at 405 nm, which was not contaminated by ORO and accurately represent ARS value. A linear regression within each group was performed and no slope was shown to be significantly different from zero, although sample sizes are small (**C**). This shows that there is no clear correlation between ARS levels and absorbance at 518 nm, indicating minimal impact of ARS contamination on ORO measurements.

Works Cited

Ab Kadir, R., Zainal Ariffin, S. H., Megat Abdul Wahab, R., Kermani, S., & Senafi, S. (2012). Characterization of Mononucleated Human Peripheral Blood Cells. *The Scientific World Journal*, *2012*. https://doi.org/10.1100/2012/843843

Abo-Aziza, F. A. M., & A.A, Z. (2017). The Impact of Confluence on Bone Marrow Mesenchymal Stem (BMMSC) Proliferation and Osteogenic Differentiation. *International Journal of Hematology-Oncology and Stem Cell Research*, *11*(2), 121–132.

Adams, D. S., & Levin, M. (2012). Measuring Resting Membrane Potential Using the Fluorescent Voltage Reporters DiBAC4(3) and CC2-DMPE. *Cold Spring Harbor Protocols*, *2012*(4), 459–464. https://doi.org/10.1101/pdb.prot067702

Assoni, A., Coatti, G., Valadares, M. C., Beccari, M., Gomes, J., Pelatti, M., … Zatz, M. (2017). Different Donors Mesenchymal Stromal Cells Secretomes Reveal Heterogeneous Profile of Relevance for Therapeutic Use. *Stem Cells and Development*, *26*(3), 206–214. https://doi.org/10.1089/scd.2016.0218

Bai, D., del Corsso, C., Srinivas, M., & Spray, D. C. (2006). Block of specific gap junction channel subtypes by 2-aminoethoxydiphenyl borate (2-APB). *The Journal of Pharmacology and Experimental Therapeutics*, *319*(3), 1452–1458. https://doi.org/10.1124/jpet.106.112045

Berndt, A., Lee, S. Y., Wietek, J., Ramakrishnan, C., Steinberg, E. E., Rashid, A. J., … Deisseroth, K. (2016). Structural foundations of optogenetics: Determinants of channelrhodopsin ion selectivity. *Proceedings of the National Academy of Sciences of the United States of America*, *113*(4), 822–829. https://doi.org/10.1073/pnas.1523341113

Betolngar, D.-B., Erard, M., Pasquier, H., Bousmah, Y., Diop-Sy, A., Guiot, E., … Mérola, F. (2015). pH sensitivity of FRET reporters based on cyan and yellow fluorescent proteins. *Analytical and Bioanalytical Chemistry*, *407*(14), 4183–4193. https://doi.org/10.1007/s00216-015-8636-z

Bhavsar, M. B., Cato, G., Hauschild, A., Leppik, L., Costa Oliveira, K. M., Eischen-Loges, M. J., & Barker, J. H. (2019). Membrane potential (V_{mem}) measurements during mesenchymal stem cell (MSC) proliferation and osteogenic differentiation. *PeerJ*, *7*, e6341. https://doi.org/10.7717/peerj.6341

Binggeli, R., & Weinstein, R. C. (1986). Membrane potentials and sodium channels: hypotheses for growth regulation and cancer formation based on changes in sodium channels and gap junctions. *Journal of Theoretical Biology*, *123*(4), 377–401.

Blackiston, D. J., McLaughlin, K. A., & Levin, M. (2009). Bioelectric controls of cell proliferation. *Cell Cycle (Georgetown, Tex.)*, *8*(21), 3519–3528.

Broussard, G. J., Liang, R., & Tian, L. (2014). Monitoring activity in neural circuits with genetically encoded indicators. *Frontiers in Molecular Neuroscience*, *7*. https://doi.org/10.3389/fnmol.2014.00097

Bukauskas, F. F., & Verselis, V. K. (2004). Gap junction channel gating. *Biochimica et Biophysica Acta*, *1662*(1–2), 42. https://doi.org/10.1016/j.bbamem.2004.01.008

Campbell, T. N., & Choy, F. (2001). The effect of pH on green fluorescent protein: A brief review. *Molecular Biology Today*, *2*, 1–4.

Cancelas, J. A., Koevoet, W. L., de Koning, A. E., Mayen, A. E., Rombouts, E. J., & Ploemacher, R. E. (2000). Connexin-43 gap junctions are involved in multiconnexin-expressing stromal support of hemopoietic progenitors and stem cells. *Blood*, *96*(2), 498–505.

Cao, J. J. (2011). Effects of obesity on bone metabolism. *Journal of Orthopaedic Surgery and Research*, *6*, 30. https://doi.org/10.1186/1749-799X-6-30

Caron, M. M. J., van der Windt, A. E., Emans, P. J., van Rhijn, L. W., Jahr, H., & Welting, T. J. M. (2013). Osmolarity determines the in vitro chondrogenic differentiation capacity of progenitor cells via nuclear factor of activated T-cells 5. *Bone*, *53*(1), 94–102. https://doi.org/10.1016/j.bone.2012.11.032

Catterall, W. A. (2011). Voltage-Gated Calcium Channels. *Cold Spring Harbor Perspectives in Biology*, *3*(8). https://doi.org/10.1101/cshperspect.a003947

Chen, Q., Shou, P., Zheng, C., Jiang, M., Cao, G., Yang, Q., … Shi, Y. (2016). Fate decision of mesenchymal stem cells: adipocytes or osteoblasts? *Cell Death and Differentiation*, *23*(7), 1128–1139. https://doi.org/10.1038/cdd.2015.168

Chernet, B. T., & Levin, M. (2013). Transmembrane voltage potential is an essential cellular parameter for the detection and control of tumor development in a Xenopus model. *Disease Models & Mechanisms*, *6*(3), 595–607. https://doi.org/10.1242/dmm.010835

Cone, C. D., & Cone, C. M. (1976). Induction of Mitosis in Mature Neurons in Central Nervous System by Sustained Depolarization. *Science*, *192*(4235), 155–158. Retrieved from JSTOR.

Dall'Asta, V., Rossi, P. A., Bussolati, O., & Gazzola, G. C. (1994). Response of human fibroblasts to hypertonic stress. Cell shrinkage is counteracted by an enhanced active transport of neutral amino acids. *The Journal of Biological Chemistry*, *269*(14), 10485–10491.

Degrelle, S. A., Shoaito, H., & Fournier, T. (2017). New Transcriptional Reporters to Quantify and Monitor PPARγ Activity. *PPAR Research*, *2017*, 6139107. https://doi.org/10.1155/2017/6139107

Dominici, M., Le Blanc, K., Mueller, I., Slaper-Cortenbach, I., Marini, F., Krause, D., … Horwitz, E. (2006). Minimal criteria for defining multipotent mesenchymal stromal cells. The International Society for Cellular Therapy position statement. *Cytotherapy*, *8*(4), 315–317. https://doi.org/10.1080/14653240600855905

Dungan, J., Mathews, J., Levin, M., & Koomson, V. (2017). Microfluidic platform to study intercellular connectivity through on-chip electrical impedance measurement. *2017 IEEE 60th International Midwest Symposium on Circuits and Systems (MWSCAS)*, 56–59. https://doi.org/10.1109/MWSCAS.2017.8052859

Duval, N., Gomès, D., Calaora, V., Calabrese, A., Meda, P., & Bruzzone, R. (2002). Cell coupling and Cx43 expression in embryonic mouse neural progenitor cells. *Journal of Cell Science*, *115*(16), 3241–3251.

Erdogan, A., Schaefer, C. A., Schaefer, M., Luedders, D. W., Stockhausen, F., Abdallah, Y., … Kuhlmann, C. R. W. (2005). Margatoxin Inhibits VEGF-Induced Hyperpolarization, Proliferation and Nitric Oxide Production of Human Endothelial Cells. *Journal of Vascular Research*, *42*(5), 368–376. https://doi.org/10.1159/000087159

Erndt-Marino, J., Trinkle, E., & Hahn, M. S. (2019). Hyperosmolar Potassium (K+) Treatment Suppresses Osteoarthritic Chondrocyte Catabolic and Inflammatory Protein

Production in a 3-Dimensional In Vitro Model. *Cartilage*, *10*(2), 186–195. https://doi.org/10.1177/1947603517734028

Figueroa, F. E., Carrión, F., Villanueva, S., & Khoury, M. (2012). Mesenchymal Stem Cell treatment for autoimmune diseases: a critical review. *Biological Research*, *45*(3), 269–277. https://doi.org/10.4067/S0716-97602012000300008

Gönczi, M., Szentandrássy, N., Fülöp, L., Telek, A., Szigeti, G. P., Magyar, J., … Csernoch, L. (2007). Hypotonic stress influence the membrane potential and alter the proliferation of keratinocytes in vitro. *Experimental Dermatology*, *16*(4), 302–310. https://doi.org/10.1111/j.1600-0625.2006.00533.x

Guo, M., Pegoraro, A. F., Mao, A., Zhou, E. H., Arany, P. R., Han, Y., … Weitz, D. A. (2017). Cell volume change through water efflux impacts cell stiffness and stem cell fate. *Proceedings of the National Academy of Sciences*, *114*(41), E8618–E8627. https://doi.org/10.1073/pnas.1705179114

Han, Y., Bai, T., & Liu, W. (2014). Controlled Heterogeneous Stem Cell Differentiation on a Shape Memory Hydrogel Surface. *Scientific Reports*, *4*, 5815. https://doi.org/10.1038/srep05815

Hervé, J.-C., & Derangeon, M. (2013). Gap-junction-mediated cell-to-cell communication. *Cell and Tissue Research*, *352*(1), 21–31. https://doi.org/10.1007/s00441-012-1485-6

Higashi, H., Katayama, Y., Morita, K., & North, R. A. (1987). Ouabain augments calcium-dependent potassium conductance in visceral primary afferent neurones of the rabbit. *The Journal of Physiology*, *389*, 629–645.

Hotary, K. B., & Robinson, K. R. (1992). Evidence of a role for endogenous electrical fields in chick embryo development. *Development (Cambridge, England)*, *114*(4), 985–996.

Hwang, N. S., Varghese, S., & Elisseeff, J. (2008). Controlled differentiation of stem cells. *Advanced Drug Delivery Reviews*, *60*(2), 199–214. https://doi.org/10.1016/j.addr.2007.08.036

Jaffe, L. F., & Nuccitelli, R. (1977). Electrical controls of development. *Annual Review of Biophysics and Bioengineering*, *6*, 445–476. https://doi.org/10.1146/annurev.bb.06.060177.002305

Jenkins, L. S., Duerstock, B. S., & Borgens, R. B. (1996). Reduction of the current of injury leaving the amputation inhibits limb regeneration in the red spotted newt. *Developmental Biology*, *178*(2), 251–262. https://doi.org/10.1006/dbio.1996.0216

Jin, L., Han, Z., Platisa, J., Wooltorton, J. R. A., Cohen, L. B., & Pieribone, V. A. (2012). Single action potentials and subthreshold electrical events imaged in neurons with a novel fluorescent protein voltage probe. *Neuron*, *75*(5), 779–785. https://doi.org/10.1016/j.neuron.2012.06.040

Kawai, M., de Paula, F. J. A., & Rosen, C. J. (2012). New Insights into Osteoporosis: The Bone-Fat Connection. *Journal of Internal Medicine*, *272*(4), 317–329. https://doi.org/10.1111/j.1365-2796.2012.02564.x

Komori, T. (2009). Regulation of bone development and extracellular matrix protein genes by RUNX2. *Cell and Tissue Research*, *339*(1), 189. https://doi.org/10.1007/s00441-009-0832-8

Konig, S., Béguet, A., Bader, C. R., & Bernheim, L. (2006). The calcineurin pathway links hyperpolarization (Kir2.1)-induced Ca2+ signals to human myoblast differentiation and fusion. *Development (Cambridge, England)*, *133*(16), 3107–3114. https://doi.org/10.1242/dev.02479

Konig, S., Hinard, V., Arnaudeau, S., Holzer, N., Potter, G., Bader, C. R., & Bernheim, L. (2004). Membrane hyperpolarization triggers myogenin and myocyte enhancer factor-2 expression during human myoblast differentiation. *The Journal of Biological Chemistry*, *279*(27), 28187–28196. https://doi.org/10.1074/jbc.M313932200

Kornreich, B. G. (2007). The patch clamp technique: principles and technical considerations. *Journal of Veterinary Cardiology: The Official Journal of the European Society of Veterinary Cardiology*, *9*(1), 25–37. https://doi.org/10.1016/j.jvc.2007.02.001

Lan, J.-Y., Williams, C., Levin, M., & Black, L. D. (2014). Depolarization of Cellular Resting Membrane Potential Promotes Neonatal Cardiomyocyte Proliferation In Vitro. *Cellular and Molecular Bioengineering*, *7*(3), 432–445. https://doi.org/10.1007/s12195-014-0346-7

Lee, H., Stowers, R., & Chaudhuri, O. (2019). Volume expansion and TRPV4 activation regulate stem cell fate in three-dimensional microenvironments. *Nature Communications*, *10*. https://doi.org/10.1038/s41467-019-08465-x

Lefterova, M. I., Haakonsson, A. K., Lazar, M. A., & Mandrup, S. (2014). PPARγ and the global map of adipogenesis and beyond. *Trends in Endocrinology & Metabolism*, *25*(6), 293–302. https://doi.org/10.1016/j.tem.2014.04.001

Levin, M. (2007). Large-scale biophysics: ion flows and regeneration. *Trends in Cell Biology*, *17*(6), 261–270. https://doi.org/10.1016/j.tcb.2007.04.007

Levin, M., & Martyniuk, C. J. (2018). The bioelectric code: An ancient computational medium for dynamic control of growth and form. *Biosystems*, *164*, 76–93. https://doi.org/10.1016/j.biosystems.2017.08.009

Levin, M., Pezzulo, G., & Finkelstein, J. M. (2017). Endogenous Bioelectric Signaling Networks: Exploiting Voltage Gradients for Control of Growth and Form. *Annual Review of Biomedical Engineering*, *19*(1), 353–387. https://doi.org/10.1146/annurev-bioeng-071114-040647

Li, W., Li, K., Wei, W., & Ding, S. (2013). Chemical approaches to stem cell biology and therapeutics. *Cell Stem Cell*, *13*(3), 270–283. https://doi.org/10.1016/j.stem.2013.08.002

Lian Qizhou, Zhang Yuelin, Zhang Jinqiu, Zhang Hua Kun, Wu Xingang, Zhang Yang, … Tse Hung-Fat. (2010). Functional Mesenchymal Stem Cells Derived From Human Induced Pluripotent Stem Cells Attenuate Limb Ischemia in Mice. *Circulation*, *121*(9), 1113–1123. https://doi.org/10.1161/CIRCULATIONAHA.109.898312

Liu, J.-H., Bijlenga, P., Fischer-Lougheed, J., Occhiodoro, T., Kaelin, A., Bader, C. R., & Bernheim, L. (1998). Role of an inward rectifier K+ current and of hyperpolarization in human myoblast fusion. *The Journal of Physiology*, *510*(Pt 2), 467–476. https://doi.org/10.1111/j.1469-7793.1998.467bk.x

Louwen, F., Ritter, A., Kreis, N. N., & Yuan, J. (2018). Insight into the development of obesity: functional alterations of adipose-derived mesenchymal stem cells. *Obesity Reviews*, *19*(7), 888–904. https://doi.org/10.1111/obr.12679

M. Ashcroft, F., & M. Gribble, F. (2000). New windows on the mechanism of action of KATP channel openers. *Trends in Pharmacological Sciences*, *21*(11), 439–445. https://doi.org/10.1016/S0165-6147(00)01563-7

Mahla, R. S. (2016). Stem Cells Applications in Regenerative Medicine and Disease Therapeutics. *International Journal of Cell Biology*, *2016*. https://doi.org/10.1155/2016/6940283

Marh, J., Stoytcheva, Z., Urschitz, J., Sugawara, A., Yamashiro, H., Owens, J. B., … Moisyadi, S. (2012). Hyperactive self-inactivating piggyBac for transposase-enhanced pronuclear microinjection transgenesis. *Proceedings of the National Academy of Sciences of the United States of America*, *109*(47), 19184–19189. https://doi.org/10.1073/pnas.1216473109

Matsumoto, S., Kitagawa, J., & Takeda, M. (2008). The effects of ouabain on resting membrane potential and hyperpolarization-activated current in neonatal rat nodose ganglion neurons. *Neuroscience Letters*, *439*(3), 241–244. https://doi.org/10.1016/j.neulet.2008.05.032

Mattis, J., Tye, K. M., Ferenczi, E. A., Ramakrishnan, C., O'Shea, D. J., Prakash, R., … Deisseroth, K. (2011). Principles for applying optogenetic tools derived from direct comparative analysis of microbial opsins. *Nature Methods*, *9*(2), 159–172. https://doi.org/10.1038/nmeth.1808

McBeath, R., Pirone, D. M., Nelson, C. M., Bhadriraju, K., & Chen, C. S. (2004). Cell shape, cytoskeletal tension, and RhoA regulate stem cell lineage commitment. *Developmental Cell*, *6*(4), 483–495.

Miesenböck, G., Angelis, D. A. D., & Rothman, J. E. (1998). Visualizing secretion and synaptic transmission with pH-sensitive green fluorescent proteins. *Nature*, *394*(6689), 192. https://doi.org/10.1038/28190

Moerman, E. J., Teng, K., Lipschitz, D. A., & Lecka-Czernik, B. (2004). Aging activates adipogenic and suppresses osteogenic programs in mesenchymal marrow stroma/stem cells: the role of PPAR-gamma2 transcription factor and TGF-beta/BMP signaling pathways. *Aging Cell*, *3*(6), 379–389. https://doi.org/10.1111/j.1474-9728.2004.00127.x

Montecino-Rodriguez, E., & Dorshkind, K. (2001). Regulation of hematopoiesis by gap junction-mediated intercellular communication. *Journal of Leukocyte Biology*, *70*(3), 341–347.

Ng, S.-Y., Chin, C.-H., Lau, Y.-T., Luo, J., Wong, C.-K., Bian, Z.-X., & Tsang, S.-Y. (2010). Role of voltage-gated potassium channels in the fate determination of embryonic stem cells. *Journal of Cellular Physiology*, *224*(1), 165–177. https://doi.org/10.1002/jcp.22113

Nielsen, M. S., Axelsen, L. N., Sorgen, P. L., Verma, V., Delmar, M., & Holstein-Rathlou, N.-H. (2012). Gap Junctions. *Comprehensive Physiology*, *2*(3). https://doi.org/10.1002/cphy.c110051

Oviedo, N. J., Morokuma, J., Walentek, P., Kema, I. P., Gu, M. B., Ahn, J.-M., … Levin, M. (2010). Long-range neural and gap junction protein-mediated cues control polarity during planarian regeneration. *Developmental Biology*, *339*(1), 188–199. https://doi.org/10.1016/j.ydbio.2009.12.012

Pai, V. P., Aw, S., Shomrat, T., Lemire, J. M., & Levin, M. (2012). Transmembrane voltage potential controls embryonic eye patterning in Xenopus laevis. *Development (Cambridge, England)*, *139*(2), 313–323. https://doi.org/10.1242/dev.073759

Pereda, A. E., Curti, S., Hoge, G., Cachope, R., Flores, C. E., & Rash, J. E. (2013). Gap junction-mediated electrical transmission: Regulatory mechanisms and plasticity. *Biochimica et Biophysica Acta (BBA) - Biomembranes*, *1828*(1), 134–146. https://doi.org/10.1016/j.bbamem.2012.05.026

Pino, A. M., Rosen, C. J., & Rodríguez, J. P. (2012). In Osteoporosis, differentiation of mesenchymal stem cells (MSCs) improves bone marrow adipogenesis. *Biological Research*, *45*(3), 279–287. https://doi.org/10.4067/S0716-97602012000300009

Pittenger, M. F., Mackay, A. M., Beck, S. C., Jaiswal, R. K., Douglas, R., Mosca, J. D., … Marshak, D. R. (1999). Multilineage Potential of Adult Human Mesenchymal Stem Cells. *Science*, *284*(5411), 143–147. https://doi.org/10.1126/science.284.5411.143

Ruch, R. J., Guan, X., & Sigler, K. (1995). Inhibition of gap junctional intercellular communication and enhancement of growth in BALB/c 3t3 cells treated with connexin43 antisense oligonucleotides. *Molecular Carcinogenesis*, *14*(4), 269–274. https://doi.org/10.1002/mc.2940140407

Ruiz, S. A., & Chen, C. S. (2008). Emergence of patterned stem cell differentiation within multicellular structures. *Stem Cells (Dayton, Ohio)*, *26*(11), 2921–2927. https://doi.org/10.1634/stemcells.2008-0432

Scott, M. A., Nguyen, V. T., Levi, B., & James, A. W. (2011). Current Methods of Adipogenic Differentiation of Mesenchymal Stem Cells. *Stem Cells and Development*, *20*(10), 1793–1804. https://doi.org/10.1089/scd.2011.0040

Slusarski, D. C., & Pelegri, F. (2007). Calcium signaling in vertebrate embryonic patterning and morphogenesis. *Developmental Biology*, *307*(1), 1–13. https://doi.org/10.1016/j.ydbio.2007.04.043

Sneyd, J., Wilkins, M., Strahonja, A., & Sanderson, M. J. (1998). Calcium waves and oscillations driven by an intercellular gradient of inositol (1,4,5)-trisphosphate. *Biophysical Chemistry*, *72*(1–2), 101–109.

Sonomoto, K., Yamaoka, K., Kaneko, H., Yamagata, K., Sakata, K., Zhang, X., … Tanaka, Y. (2016). Spontaneous Differentiation of Human Mesenchymal Stem Cells on Poly-Lactic-Co-Glycolic Acid Nano-Fiber Scaffold. *PLoS ONE*, *11*(4). https://doi.org/10.1371/journal.pone.0153231

Stagg, J. (2007). Immune regulation by mesenchymal stem cells: two sides to the coin. *Tissue Antigens*, *69*(1), 1–9. https://doi.org/10.1111/j.1399-0039.2006.00739.x

Sun, Y., Chen, C. S., & Fu, J. (2012). Forcing stem cells to behave: a biophysical perspective of the cellular microenvironment. *Annual Review of Biophysics*, *41*, 519–542. https://doi.org/10.1146/annurev-biophys-042910-155306

Sundelacruz, S., Levin, M., & Kaplan, D. L. (2008). Membrane Potential Controls Adipogenic and Osteogenic Differentiation of Mesenchymal Stem Cells. *PLoS ONE*, *3*(11). https://doi.org/10.1371/journal.pone.0003737

Sundelacruz, S., Levin, M., & Kaplan, D. L. (2009). Role of Membrane Potential in the Regulation of Cell Proliferation and Differentiation. *Stem Cell Reviews and Reports*, *5*(3), 231–246. https://doi.org/10.1007/s12015-009-9080-2

Sundelacruz, S., Levin, M., & Kaplan, D. L. (2013). Depolarization Alters Phenotype, Maintains Plasticity of Predifferentiated Mesenchymal Stem Cells. *Tissue Engineering. Part A*, *19*(17–18), 1889–1908. https://doi.org/10.1089/ten.tea.2012.0425.rev

Sundelacruz, S., Moody, A. T., Levin, M., & Kaplan, D. L. (2019). Membrane Potential Depolarization Alters Calcium Flux and Phosphate Signaling During Osteogenic Differentiation of Human Mesenchymal Stem Cells. *Bioelectricity*, *1*(1), 56–66. https://doi.org/10.1089/bioe.2018.0005

Takahashi, K., Tanabe, K., Ohnuki, M., Narita, M., Ichisaka, T., Tomoda, K., & Yamanaka, S. (2007). Induction of pluripotent stem cells from adult human fibroblasts by defined factors. *Cell*, *131*(5), 861–872. https://doi.org/10.1016/j.cell.2007.11.019

Todorova, M. G., Soria, B., & Quesada, I. (2008). Gap junctional intercellular communication is required to maintain embryonic stem cells in a non-differentiated and proliferative state. *Journal of Cellular Physiology*, *214*(2), 354–362. https://doi.org/10.1002/jcp.21203

Tsutsui, H., Jinno, Y., Tomita, A., Niino, Y., Yamada, Y., Mikoshiba, K., … Okamura, Y. (2013). Improved detection of electrical activity with a voltage probe based on a voltage-sensing phosphatase. *The Journal of Physiology*, *591*(Pt 18), 4427–4437. https://doi.org/10.1113/jphysiol.2013.257048

Valiunas, V., Doronin, S., Valiuniene, L., Potapova, I., Zuckerman, J., Walcott, B., … Cohen, I. S. (2004). Human mesenchymal stem cells make cardiac connexins and form functional gap junctions. *The Journal of Physiology*, *555*(Pt 3), 617–626. https://doi.org/10.1113/jphysiol.2003.058719

Villars, F., Guillotin, B., Amédée, T., Dutoya, S., Bordenave, L., Bareille, R., & Amédée, J. (2002). Effect of HUVEC on human osteoprogenitor cell differentiation needs heterotypic gap junction communication. *American Journal of Physiology-Cell Physiology*, *282*(4), C775–C785. https://doi.org/10.1152/ajpcell.00310.2001

Vitali, I., Fièvre, S., Telley, L., Oberst, P., Bariselli, S., Frangeul, L., … Jabaudon, D. (2018). Progenitor Hyperpolarization Regulates the Sequential Generation of Neuronal Subtypes in the Developing Neocortex. *Cell*, *174*(5), 1264-1276.e15. https://doi.org/10.1016/j.cell.2018.06.036

Wagner, W., Wein, F., Seckinger, A., Frankhauser, M., Wirkner, U., Krause, U., … Ho, A. D. (2005). Comparative characteristics of mesenchymal stem cells from human bone marrow, adipose tissue, and umbilical cord blood. *Experimental Hematology*, *33*(11), 1402–1416. https://doi.org/10.1016/j.exphem.2005.07.003

Wegmeyer, H., Bröske, A.-M., Leddin, M., Kuentzer, K., Nisslbeck, A. K., Hupfeld, J., … Neubauer, M. (2013). Mesenchymal Stromal Cell Characteristics Vary Depending on Their Origin. *Stem Cells and Development*, *22*(19), 2606–2618. https://doi.org/10.1089/scd.2013.0016

Xu, Y., Zou, P., & Cohen, A. E. (2017). Voltage imaging with genetically encoded indicators. *Current Opinion in Chemical Biology*, *39*, 1–10. https://doi.org/10.1016/j.cbpa.2017.04.005

Yang, H. H., & St-Pierre, F. (2016). Genetically Encoded Voltage Indicators: Opportunities and Challenges. *The Journal of Neuroscience*, *36*(39), 9977–9989. https://doi.org/10.1523/JNEUROSCI.1095-16.2016

Yizhar, O., Fenno, L. E., Prigge, M., Schneider, F., Davidson, T. J., O'Shea, D. J., … Deisseroth, K. (2011). Neocortical excitation/inhibition balance in information processing and social dysfunction. *Nature*, *477*(7363), 171–178. https://doi.org/10.1038/nature10360

Zhao, Y., Araki, S., Wu, J., Teramoto, T., Chang, Y.-F., Nakano, M., … Campbell, R. E. (2011). An Expanded Palette of Genetically Encoded Ca2+ Indicators. *Science (New York, N.Y.)*, *333*(6051), 1888–1891. https://doi.org/10.1126/science.1208592

Zhu, S., Wei, W., & Ding, S. (2011). Chemical strategies for stem cell biology and regenerative medicine. *Annual Review of Biomedical Engineering*, *13*, 73–90. https://doi.org/10.1146/annurev-bioeng-071910-124715

Zou, L., Kidwai, F. K., Kopher, R. A., Motl, J., Kellum, C. A., Westendorf, J. J., & Kaufman, D. S. (2015). Use of RUNX2 Expression to Identify Osteogenic Progenitor Cells Derived from Human Embryonic Stem Cells. *Stem Cell Reports*, *4*(2), 190–198. https://doi.org/10.1016/j.stemcr.2015.01.008